Series in Soft Condensed Matter **Vol. 2**

POLYMERS, LIQUIDS AND COLLOIDS IN ELECTRIC FIELDS

Tsori
Steiner

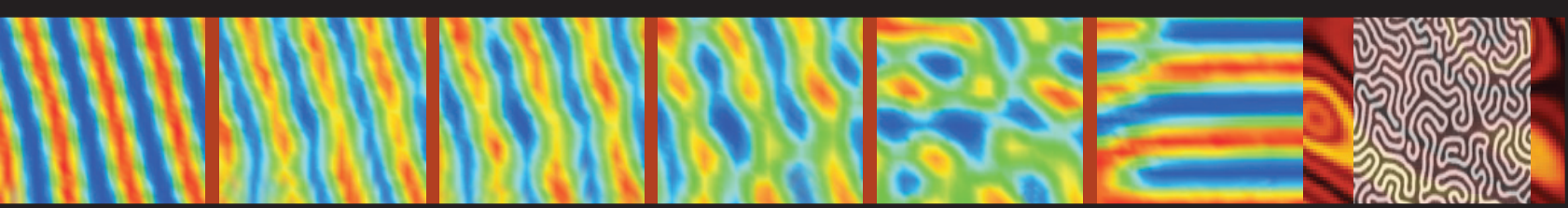

Series in Soft Condensed Matter **Vol. 2**

This unique book aims to expose the reader to a wide range of phenomena occurring when soft matter systems are put under the influence of an external electric field. The book shows how an electric field can be used to affect objects at the submicron scale, and how it controls the phase behavior of liquids and polymers. The main focus is on the basic underlying mechanisms. Some technological applications are dealt with as well.

Book chapters are arranged in a logical order, from "simple" systems to more complicated ones. In addition, each topic is covered by the mixed bag of theory, experiment and simulation; and this will give the reader a broad perspective of the underlying physical phenomena.

World Scientific
www.worldscientific.com
7266 hc

ISBN-13 978-981-4271-68-4
ISBN-10 981-4271-68-3

POLYMERS, LIQUIDS AND COLLOIDS IN ELECTRIC FIELDS

Editors
Yoav Tsori • Ullrich Steiner

POLYMERS, LIQUIDS AND COLLOIDS IN ELECTRIC FIELDS

Interfacial Instabilities, Orientation and Phase Transitions

Published in: "Polymers, Liquids and Colloids in Electric Fields: Interfacial instabilities, orientation, and phase-transitions", Eds. Y. Tsori and U. Steiner, Vol. 2 in the "Series in Soft Condensed Matter", World Scientific (2009).

Chapter 1

The Phenomenology of Modulated Phases: From Magnetic Solids and Fluids to Organic Films and Polymers*

David Andelman

The Raymond and Beverly Sackler School of Physics and Astronomy
Tel Aviv University, Ramat Aviv 69978, Tel Aviv, Israel

Ronald E. Rosensweig

34 Gloucester Rd., Summit, NJ 07901, USA

This chapter surveys aspects of patternings that occur in a wide array of physical systems due to interacting combinations of dipolar, interfacial, charge exchange, entropic, and geometric influences. We review well-established phenomena as a basis for discussion of more recent developments. While the materials of interest range from bulk inorganic solids and polymer organic melts to fluid colloids and granular suspensions, we note that often there are unifying principles behind the various modulated structures, such as the competition between surface or line tension and dipolar interaction in thermally reversible systems; their properties can be understood by free-energy minimization. In other cases, the patterns are determined by dissipative forces. In all these systems the patterning is modulated by the application of force fields. Another common feature of these disparate systems is that a phase diagram often emerges as a convenient descriptor. We also mention a number of interesting technological applications for certain of the systems under review.

1. Introduction

A large number of diverse physical systems manifest some type of modulation in their structural properties.[1] Examples of such structures in

*This chapter is dedicated to the memory of Pierre-Gilles de Gennes, 1932-2007, a great scientist and close friend, who, with his characteristic gleefulness and insight, stimulated and supported us in our own studies.

Table 1. Table of Symbols

Symbol	Definition	Units
a	microscopic length	m
B	$= \mu_0(H + M)$, magnetic induction	tesla
d	particle diameter	m
d^*	domain size of modulated phase	m
d_0	domain size of BCP system	m
D	demagnetization coefficient	dimensionless
E	electric field	$\mathrm{m\,kg/s^3 ampere}$
f_p	free energy per particle	joule
$\mathcal{F}_d$	dipolar layer free energy	joule
f_A	mole fraction of the A monomers	dimensionless
g	acceleration of gravity	$\mathrm{m/s^2}$
$g(r)$	kernel in Eq. (3)	$1/\mathrm{m^3}$
$G(q)$	2D Fourier transform of $g(r)$	1/m
g_1	linear coefficient in the expansion of $G(q)$ in Eq. (4)	dimensionless
H	magnetic field magnitude	ampere/m
k_B	Boltzmann constant	joule/kelvin
m	$= \mu_0 MV$ magnetic moment	$\mathrm{tesla\,m^3}$
M	magnetization	ampere/m
$\mathcal{M}$	2D magnetization as in Sec. 3	ampere
$\mathcal{M}_q$	Fourier component of the 2D magnetization	$\mathrm{ampere\ m^2}$
n	particle number density	$1/\mathrm{m^3}$
N_A	number of monomers of the A block on the chain	dimensionless
N_B	number of monomers of the B block on the chain	dimensionless
N	$= N_A + N_B$; total length of polymer chain	dimensionless
N_{B_0}	magnetic Bond number	dimensionless
P	electric polarization	$\mathrm{ampere\ s/m^2}$
q	wavenumber	1/m
r	distance between dipoles	m
r_d	center to center distance between particles	m
t	sample thickness in the z-direction	m
T	temperature	kelvin
T_c	critical (Curie) temperature	kelvin
V	volume	$\mathrm{m^3}$
μ	$= (\partial nf/\partial n)_{H,T}$; chemical potential per particle	joule
μ_0	permeability of vacuum	henry/m
ρ_m	mass density	$\mathrm{kg/m^3}$
σ	interfacial tension	newton/m
χ	magnetic susceptibility	dimensionless
χ_{AB}	Flory constant for polymers	dimensionless
ε	dielectric constant	$\mathrm{ampere^2 s^4/m^3 kg}$
γ	domain wall energy or line tension (in 2D)	joule/m
$\phi(r)$	local volume fraction in an A-B di-block copolymer	dimensionless

$\mathrm{tesla{=}kg\,s^{-2}\,ampere;\ henry{=}m^2\,kg\,s^{-2}ampere^2;}$ joule=newton m; $\mathrm{newton{=}kg\,m\,s^{-2}}$

two-dimensional (2D) systems are elongated stripes and compact droplet-like domains as can be seen in Fig. 1. In the figure, domains in solid magnetic systems (garnet films) and in thin layers of ferrofluids (to be discussed in detail below) are shown side-by-side and exhibit striking similarity. In three dimensional (3D) systems, the domain morphology can be more complex and includes sheets, tubes, rods and droplets embedded in a three-dimensional matrix. The similarity between the resulting patterns in systems of different origins is quite surprising and may allude to a common unifying mechanism.

An approach we adopt here is to view these systems as a manifestation of modulated phases, i.e. systems which, due to a competition between different interactions, achieve thermodynamic equilibrium in a state in which

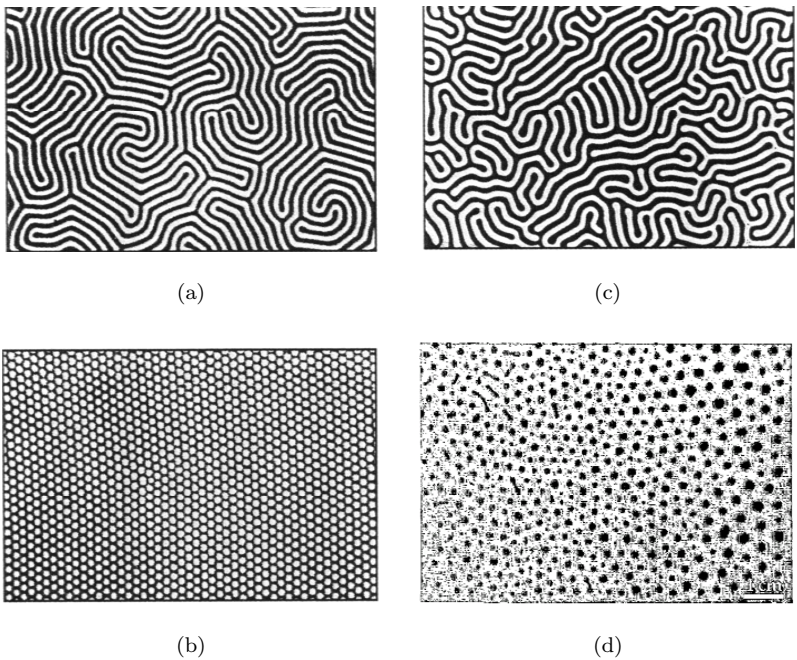

Fig. 1. Domains in magnetic solids and fluids. (a) stripes and (b) bubble phase in ferromagnetic garnet film of 13 μm thickness grown on $\langle 111 \rangle$ face of gadolinium gallium garnet. Visualization in made using polarized optical microscopy (Faraday effect). Period $d^* \sim 10\,\mu$m. Adapted from Ref. 2. (c) Ferrofluid confined between two glass plates exhibiting labyrinthine instability in a magnetic field.[3,4] The period is $d^* \sim 2$ mm. (d) Bubble phase of a ferrofluid confined in a cell having a gap that increases from left to right. The mean bubble size is ~ 1 mm. Adapted from Ref. 5.

the appropriate order parameter shows a spatial modulation. Examples are abundant[1] and include modulation of the magnetization field of ferromagnetic slabs[6–8] and ferrofluids,[3] polarization field in electric dipolar systems and certain liquid crystalline phases,[9,10] the superconducting order parameter in the intermediate phase of type I superconductors,[11] as well as the relative composition in block copolymer systems.[12–14]

Thus, in this chapter we review some of the interesting phenomena associated with modulated phases. We start by considering a simple example explaining the underlying mechanism of wavelength selection in a quasi two-dimensional dipolar system. We then review domains in related dipolar organic films on water/air interface (Langmuir monolayers) and magnetic garnet films. Two other examples of systems of current scientific interest having many applications are subsequently discussed: magnetic fluids (ferrofluids) and mesophases in block copolymers. We review how the competing interactions create interesting new phenomena when these systems are subjected to an external field (electric, magnetic) and describe their morphology, structure, phase separation, various instabilities and related phenomena. In addition, certain systems of granular suspensions are discussed having structures that are modulated by the application of forces such as magnetic attraction and viscous drag.

A table of symbols is given at the beginning of this chapter.

2. Domains in Magnetic Solids

Ferromagnetism[15] is an important physical phenomenon associated with elements like nickel, iron and cobalt, as well as a large number of metallic alloys that show spontaneous magnetization M in the absence of external applied magnetic field. The reason for a macroscopic magnetization is deeply rooted in the existence of electronic spin $\mathbf{S}_i$ associated with an atom at position i, and the strong direct exchange interactions of the type $-J\mathbf{S}_i \cdot \mathbf{S}_j$ where J is the direct exchange integral. It is positive for ferromagnetic coupling and is related to the overlap in the charge distribution of the two neighboring atoms (i,j). The magnetization is temperature dependent. In the absence of an H field, as the temperature T is increased, the system gradually loses its magnetization, $M(T, H{=}0)$, until at a special temperature, T_c, called the *Curie temperature*, the spontaneous magnetization drops to zero, $M{=}0$.

In bulk magnetic systems, the uniform magnetization does not persist throughout the system but breaks up into spatial domains , each having a

specific and distinct magnetic orientation. P.-E. Weiss in 1907 first introduced the concept of these magnetic domains.[16] Study of the phenomenon has a long history including the notable analysis of Landau and Lifshitz in the 1930s[17] [See also Refs. 18,19]. The domain size and its structure depend on competing interactions inside the magnet: the direct exchange interaction, the demagnetization fields and the crystal anisotropy. In order to explain on general grounds why dipolar systems prefer to break into domains of a well-defined size, we use the following simplified model, which gives the essential features without the need to review all the technical details.[1,10] This model is applied in later sections to explain analogous features of magnetic garnet and films and dipolar Langmuir layers and is related to the labyrinthine instability of ferrofluids, as will be discussed below.

3. Domains in Two-Dimensional Ferromagnetic Layers

Consider a monomolecular layer of atomic dipoles in the (x,y) plane, each having a magnetic dipole (electronic spin) that can only point along the perpendicular z–direction. We assume that the spins possess two possible values: $S^z = \pm 1/2$, related to the two values of the atomic magnetic moment $m = g_0 \mu_B S^z$, where $g_0 \mu_B$ is the gyromagnetic factor, $\mu_B = e\hbar/2m_e c$ is the Bohr magneton and $g_0 \approx 2$ is the g-factor. The system can be described using an Ising model with nearest-neighbor-only ferromagnetic coupling, and the direct exchange interaction between adjacent spins minimized when two neighboring spins point in the same direction. Therefore, at low enough temperatures the magnetic order will be ferromagnetic; i.e. the spins prefer to be aligned in the same orientation even in the absence of an external field.

By treating the Ising monolayer defined above at a coarse-grained level, we can perform the thermal average; namely, to sum with the proper Boltzmann weight factor over the microscopic spin degrees of freedom at finite temperatures. A local magnetization field for this 2D system, $\mathcal{M}(\mathbf{r})$ can be defined as a continuous function of the 2D position $\mathbf{r}$. Close to the Curie temperature T_c and at zero applied magnetic field H, the magnetization is small and the ferromagnetic ($\mathcal{M}\neq 0$) to paramagnetic ($\mathcal{M}=0$) transition can be described by an expansion of the free energy expressed in powers of $\mathcal{M}$ and its gradient. This is the starting point of the well-known Ginzburg-Landau theory.[20] Because of the up-down spin symmetry in the absence of an orienting field, an expansion of the free energy has only even powers in

$\mathcal{M}$, and up to fourth order in $\mathcal{M}$ it can be written as:

$$\mathcal{F}_{\rm GL} = \int d^2\mathbf{r} \left[\frac{c}{2}|\nabla\mathcal{M}|^2 + \frac{\alpha}{2}\mathcal{M}^2(\mathbf{r}) + \frac{\beta}{4}\mathcal{M}^4(\mathbf{r})\right] \tag{1}$$

The parameter c (related to the direct exchange interaction), $\alpha \sim T - T_c$ and β are phenomenological parameters. The uniform state of the system, in which the magnetization is independent of position can be obtained from $\mathcal{F}_{\rm GL}$ by minimizing the integrand without the gradient term. This is known as the Landau theory. For $T < T_c$, the minimization yields two possible ferromagnetic states, $\mathcal{M}(T) = \pm\mathcal{M}_0 = \pm\sqrt{|\alpha|/\beta}$, while for $T > T_c$, the only solution is the paramagnetic state, $\mathcal{M} = 0$.

Any two magnetic spins also have a dipolar interaction leading to demagnetization terms which need to be included in the free energy. We consider the addition of these long-range interactions for Ising spins because these interactions have an important effect on the magnetic domain size. The dipolar interaction between any two colinear Ising spins, S_i^z and S_j^z, that point in the z-direction with possible values $\pm 1/2$, are located in the (x,y) plane, and separated by a distance r is

$$U_{i,j} = \frac{m_i m_j}{4\pi\mu_0 r^3} = \frac{(g_0\mu_B)^2}{4\pi\mu_0}\frac{S_i^z S_j^z}{r^3} \tag{2}$$

where $m_i = g_0\mu_B S_i^z$ is the atomic magnetic moment and μ_0 the vacuum permeability. We recall that the energy for a parallel pair is repulsive ($U > 0$), while that of an anti-parallel pair is attractive ($U < 0$).

The coarse-grained dipolar magnetic energy can be derived from Eq. (2) and after thermal averaging is written as:

$$\mathcal{F}_d = \frac{\mu_0}{8\pi}\int d^2\mathbf{r}\, d^2\mathbf{r}'\, \mathcal{M}(\mathbf{r}) g(\mathbf{r},\mathbf{r}') \mathcal{M}(\mathbf{r}') \tag{3}$$

where the double integral is taken over all possible dipole pairs. The $\frac{1}{2}$ prefactor is included in order to avoid double counting of pairs. The kernel $g(\mathbf{r},\mathbf{r}') = 1/|\mathbf{r}-\mathbf{r}'|^3$ expresses the long-range nature of the dipole-dipole interaction, Eq. (2). The integral in Eq. (3) can subsequently be manipulated more conveniently in Fourier space. Using $\mathcal{M}_q$ and $G(q)$ as the 2D Fourier transform of $\mathcal{M}(\mathbf{r})$ and $g(r)$, respectively, we obtain

$$\mathcal{F}_d = \frac{\mu_0}{32\pi^3}\int d^2\mathbf{q}\, \mathcal{M}_q G(q) \mathcal{M}_{-q} \approx -\frac{\mu_0}{32\pi^3} g_1 \int d^2\mathbf{q}\, |q|\, \mathcal{M}_q \mathcal{M}_{-q} \tag{4}$$

Because $g(r) = 1/r^3$, where $r = |\mathbf{r}|$ is the vectorial magnitude, the small q behavior of its Fourier transform $G(q) = \int d^2\mathbf{r}\, g(r) \exp(-i\mathbf{q}\cdot\mathbf{r})$ is

$G(q) \approx -g_1|q|$, and a lower length cutoff, $r = a$, has to be introduced in the integration of Eq. (4) in order to take care of the diverging of $g(r) = 1/r^3$ at $r \to 0$. We note that this cutoff has no other effect on the small q dependence of Eq. (4).

With H=0, a ferromagnetic state is described by a uniform magnetization, $\mathcal{M} = const.$, while a paramagnetic one by a zero magnetization, $\mathcal{M} = 0$. These two states can be considered as the limit of zero q-mode. But is it possible to stabilize a non-zero q-mode in the layered system? Clearly the gradient square term in Eq. (1) opposes any such modulations. The Fourier transform of the $|\nabla\mathcal{M}|^2$ term yields a positive contribution that is proportional to $q^2\mathcal{M}_q^2$, whose minimum is always attained for $q = 0$ (uniform state). However, the dipolar-dipolar term in Eq. (4) favors short wavelength modulations (high q-modes) due to the reduction in dipolar energy when the spin pair is in an anti-parallel state. The combined free energy, $\mathcal{F}_d + \mathcal{F}_{\rm GL}$, includes the direct exchange, Eq. (1), as well as the long-range dipole-dipole interactions, Eq. (4). Representing the total free energy as an integral in Fourier space, its minimization with respect to q gives the most stable mode,[10] $q = q^*$

$$\frac{d}{dq}\left(\frac{\mu_0}{32\pi^3}G(q) + cq^2\right) = 0 \quad \Rightarrow \quad q^* = -\frac{\mu_0 dG/dq}{64\pi^3 c} \simeq \frac{\mu_0}{64\pi^3}\frac{g_1}{c} > 0 \quad (5)$$

Some remarks are in order. In the derivation of q^* in Eq. (5) we neglected 4^{th} order and higher terms in the free energy, Eq. (1). Estimating the free energy by its value at q^* is called the *single-mode approximation*. It can be justified for $T \lesssim T_c$, where the most dominant q^*-mode contribution is a good approximation for the entire free energy.[21] Note that for a single q-mode, the domain size by definition is $d^* = 2\pi/q^*$. Up to a numerical prefactor, the domain wall width ξ is approximately equal to d^*. This is indeed characteristic to domains close to the critical point. Their domain wall is not sharp and ξ can be substantially larger than atomic length scales.

As the temperature is lowered and becomes considerably lower than T_c, the system cannot be described any longer within the single-mode approximation. Domains still prevail but their wall width ξ (of order of nanometers) becomes much smaller than the domain size d^* (micrometers). The domain wall energy γ (per unit length) can be calculated and depends mainly on the short-ranged, direct exchange interaction. At low temperatures, an estimate of d^* includes many q-modes and can be done for stripes, circular and other simple arrangement of domains. By considering an alternating arrangement of $\pm\mathcal{M}$ stripe domains, the dipolar energy Eq. (3) can be

calculated exactly. It includes logarithmic corrections related to magnetic fringe fields in 2D. This energy competes with the domain wall energy, which favors as few domains as possible. These two competing interactions[10] give in 2D

$$d^* = \frac{2\pi}{q^*} \simeq a \exp\left[\frac{b\gamma}{2}\frac{1}{\mu_0 \mathcal{M}^2}\right] = a \exp\left[\frac{b}{2} N_{B_0}^{-1}\right] \tag{6}$$

where a is a microscopic length and b is dimensionless prefactor. The dimensionless number $N_{B_0} = \mu_0 \mathcal{M}^2/\gamma$ is called the magnetic Bond number and is also discussed in Sec. 7. We note that d^* has a complicated dependence on temperature and magnetic field, but we do not further discuss it in this chapter.

The same Bond number that fixes the domain size, is also instrumental in understanding various instabilities of isolated drop-like domains, such as domain division and elongation, and tip splitting.[1]

4. Dipolar Langmuir Films

A manifestation of a 2D layer of dipoles can be achieved by spreading amphiphilic molecules at the water-air interface.[9,10,22] Although the dipoles are electric ones, the treatment of the long-range dipole–dipole interaction is similar to the one discussed in the preceding section for dipoles having a non-zero contribution along the perpendicular z direction. We simply need to replace the magnetic field by an electric one, and the magnetization by the electric polarization. The variation in the polarization $\mathbf{P} = P\hat{\mathbf{z}}$ is related to the variation in the local concentration: $P = \mu_{\rm el} n$, where P is the polarization, $\mu_{\rm el}$ the electric dipole moment of an individual molecule and $n(r)$ the local number concentration of dipoles (per unit area).

Amphiphilic molecules have a hydrophobic tail and a hydrophilic head that is either charged or dipolar. When these molecules are highly insoluble in the water, they form a Langmuir monolayer — a monomolecular layer that is spread at the air-water interface.[23] The layer thermodynamics can be controlled by regulating the temperature or applying a surface (in-plane) pressure.

Visualization of domains in the micrometer range is done by fluorescence optical and Brewster angle microscopies,[22] while ordered lipid domains is studied using small angle X-ray scattering (SAXS).[24] One predicts various thermodynamic states of the system as a function of temperature T and lateral pressure Π, in analogy with the gas, liquid, and solid phases in 3D

systems. In some cases, domains of various shapes and morphologies appear to be stable over long time scales.

When the molecular dipole is large, the selection of a preferred domain size can be largely attributed to the competition between dipolar interactions and the domain line tension γ. This selection is analogous with the pattern selection as discussed in the previous sections. For example, we show in Fig. 2 the domain structure of an alkyl lipid forming a Langmuir monolayer,[25] and compared it with a fluoro-alkylated lipids where most of the alkyl groups are replaced by fluorinated ones, Fig. 3(a). Due to the large dipole associated with the CF_3 chain extremity, the domain size of the fluorinated lipids is much smaller than that of hydrogenated lipids.

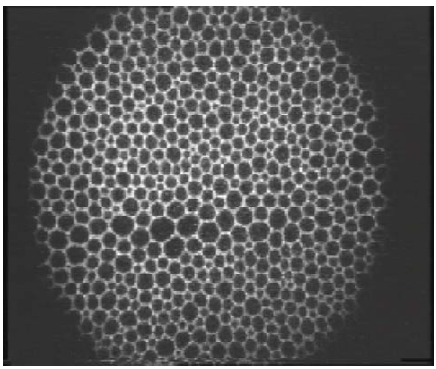

Fig. 2. Fluorescence microscopy of alkyl lipid monolayers at $T = 20°\mathrm{C}$ and area per molecule of 60Å^2 showing 2D gas-liquid coexistence. The outer circle has a diameter of $\sim 240\,\mu$m. Adapted from Ref. 25.

We mention one set of experiments indicating that the observed patterns are due to an equilibrium q-mode selection as we have discussed above. In a Langmuir monolayer formed by the phospholipid DPPC,[22] liquid-crystalline domains are seen. They take the shape of a network of elongated stripe-like structures embedded in a liquid-like background. It is known that cholesterol preferentially adsorbs to the domain perimeter and reduces the line tension γ between the domains and their liquid-like background.[22] Indeed, when cholesterol was added to the DPPC monolayer, the system quickly reduced the domain width to another characteristic width. This experimental observation is in accord with the theoretical prediction, Eq. (6), where a reduction in γ strongly reduces the size of d^*. The effect

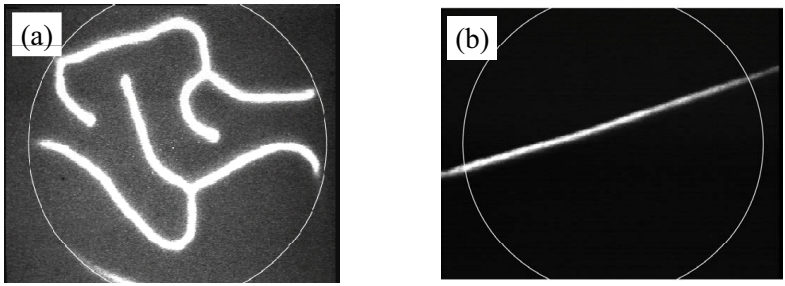

Fig. 3. (a) Partially fluoro-alkylated lipid monolayers at the same temperature and with area per molecule of 97Å^2 showing stripe-like domains with stripe thickness around 5-8 μm. (b) Same setup as in (a) but with the addition of 0.1% mol of cholesterol. A noticeable thinning of the stripe is seen to about $\sim 1-3\,\mu$m. The outer circle has a diameter of $\sim 240\,\mu$m in all figure parts. Adapted from Ref. 25.

of cholesterol was studied also for fluorinated lipids in Ref. 25. Addition of a small amount of 0.1% mol of cholesterol thins the fluoro-alkylated stripes by a large factor, as can be seen in Fig. 3(b).

Some of the problems in understanding the thermodynamics of Langmuir monolayers are related to their slow kinetics. In some cases, it is not clear whether the system reached its equilibrium state or is trapped in a long-lived metastable one. Thus, although dipoles play an important role in determining domain size and morphology, their precise role is not fully understood.

5. Magnetic Garnet Films

A well-studied system that exhibits a domain structure arising from competing energies is a magnetic garnet film . The theoretical ideas date back to the 1930's with the pioneering work[17] of Landau and Lifshitz and their related work on the *intermediate* phase of type I superconductors.[11] Garnet films had their days of glory in the 1960s and 1970s when they were used as magnetic storage devices ('bubble memory'), but their larger size and slower speed compared to hard disk drives and flash memory devices made this application short-lived.[7,19] However, even current research on meso– and nano–magnetism is largely inspired by the garnet films[8] and is briefly reviewed below.

Garnet films are ferromagnetic solid films grown so that the easy axis of magnetization is along the axis of growth.[6] The magnetic spin can point

'up' or 'down'. Using polarized light microscopy coupled to the spin orientation (via the Faraday effect) to visualize details on the micrometer scale, it is observed that below the Curie temperature the film spontaneously forms domains with a disordered stripe morphology [see Fig. 1(a)]. It is quite evident that the stripe thickness (domain size) is well defined even though the stripes have no preferred orientation in the plane. Note that for larger external fields the garnet film morphology changes into a 'bubble' phase [see Fig. 1(b)], as will be discussed below in Sec. 5.1.

The physics behind the creation of domains in garnet films, and in particular their preferred size d^* is well understood,[6,7,26] and closely related to the model 2D layered system presented in Sec. 3 above. The major difference between the two is that the garnet film has a slab geometry of finite thickness t.

Any magnetized body of finite size produces magnetic charges or poles at its surface. This surface charge distribution, acting in isolation, is itself another source of a magnetic field, called the demagnetizing field. It is called the demagnetizing field because it acts in opposition to the magnetization that produces it. Consequently, the coarse-grained dipolar magnetic energy as in Eq. (3) can be calculated by mapping the system into a Coulomb interaction between two monolayers of opposite 'charges' separated by a distance t. The kernel appearing in Eq. (3) is now replaced by[26]

$$g(r) \sim \frac{2}{r} - \frac{2}{\sqrt{r^2 + t^2}} \tag{7}$$

and the corresponding Fourier transform is

$$G(q) \sim \frac{4\pi}{qt}\left(1 - \exp(-qt)\right) \tag{8}$$

As in Sec. 3, the minimization of the free energy of Eq. (5) with the form of $G(q)$ given by Eq. (8) yields an optimal value of the modulation wavevector, q^*. The connection between the finite thickness slab of the garnet and the 2D monomolecular dipolar layer can be seen by examining the $qt \ll 1$ limit, where we find that $G(q) \sim -|q|$ as in Eq. (4). In the other limit of a thick slab, $qt \gg 1$, $G(q) \sim 1/q$, which also gives rise to a free–energy minimum at a non-zero value of q^*. The calculation of the demagnetizing field can also be done in another way. It is sensitive to the technique used to sum over the microscopic scale (lattice of atomic dipoles) and how the coarse-graining is done. The results in the small

q limit should all converge to the same continuum description. For the opposite large q (small r) limit, different ways of introducing a microscopic cutoff are employed, but these have no qualitative effect on the free energy.

Stripe-like domains can be stabilized even for zero applied magnetic field where there is a complete symmetry between the up and down spin orientations. In a slab of thickness t in the micrometer range, the resulting demagnetizing fields are strong enough to compete with the magnetic wall energy, and yield stable stripe-like domains with size d^* in the 1-100 micrometer range. Beside its dependence on the slab thickness t, the stripe width d^* depends on the temperature.

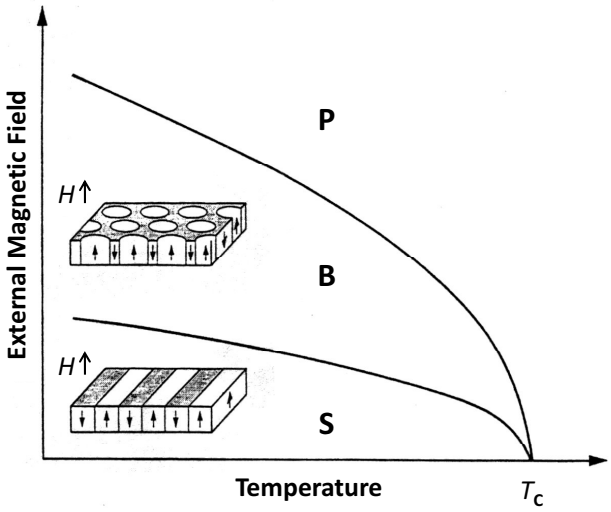

Fig. 4. Schematic phase diagram of modulated phases (garnet films). The 2D system exhibits stripe (S) and bubble (B) phases, along with the usual paramagnetic (P) phase in the temperature-field ($T-H$) plane. The lines indicate first-order transition lines from S to B and then from the B to P phase. Both lines merge at the Curie point T_c for H=0. Also indicated is the geometry of the stripe and bubble arrays for magnetic garnet films. Arrows indicate the magnetization direction. Adapted from Ref. 26.

5.1. *Phase transitions*

The phase diagram of the garnet is shown in Fig. 4 and depends on temperature and external magnetic field (for a fixed slab thickness t). For $H = 0$, the up and down stripes are completely symmetric. When an external field

is applied below the Curie temperature, the domains whose magnetization is parallel to the field direction grow at the expense of the oppositely oriented domains. But at some value of H, there is a first-order phase transition between the stripe morphology (S) and the so-called 'bubble' phase (B), as seen in Fig. 4. The bubble phase is composed of thin cylinders of up spin embedded in a background of down spins.

Upon further increase of the magnetic field, the system has another first-order phase transition from the bubble phase into a paramagnetic (P) phase. Note that the two transition lines: S$\rightarrow$ B and B$\rightarrow$ P terminate at the Curie temperature T_c, for $H = 0$. Although the periodicity is by and large determined by such equilibrium considerations, the system shows a wide range of in-plane disorder [Fig. 1(a) and (c)]. This disorder is very sensitive to the sample history indicating that care be taken to avoid trapping the system in metastable states. A sample cooled in a non-zero H field which is then removed, shows different disorder compared with a sample annealed at the same temperature but at zero magnetic field.

6. Mesomagnetism and Nanomagnetism

Mesomagnetism and nanomagnetism refer to domain structures in certain solid state magnetic materials and composites having small dimensions, e.g. thin magnetic films[8] with thickness in the submicron range, see Fig. 5. These magnetic systems are to be compared with ferromagnetic garnet and ferrofluid films where the domain size and thickness are much larger, Fig. 1.

The spatial modulations in these materials correspond as usual to minimum energy configurations. But in addition to the contributions of magnetic field and surface energy terms, one must also include the effects of the exchange and anisotropy energies. Exchange energy arises from the presence of electron spins as noted earlier, and anisotropy energy arises from the presence of a finite angle between magnetization and the crystalline axis. These energies govern the thickness of a domain wall, and when the sample size is small enough to be comparable with the wall thickness new phenomena arise including electron spin effects. A convenient method to control the sample size is by using thin films, in which only one dimension of the sample is small. Wires with two small lateral dimensions are also studied.

Electrons carry charge and spin but conventional electronics employs only the transport of charge (current). In the newly developed field of

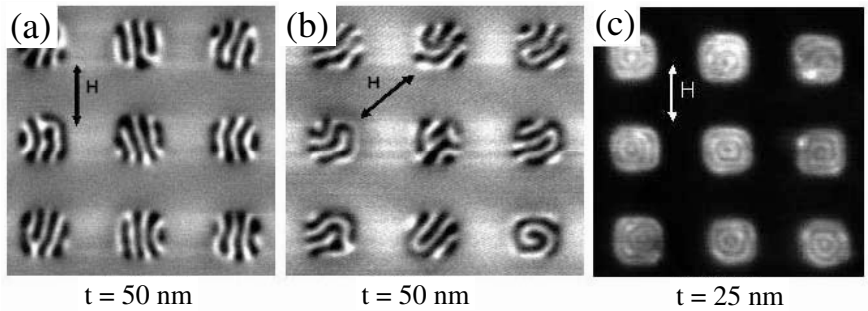

Fig. 5. Examples of induced stripe domains $\sim 0.5\,\mu$m wide in epitaxial cobalt dots 50 nm thick. (a) Field applied parallel to the edge of the square dot, and; (b) along the diagonal as indicated by the H vector. (c) Circular stripe domains induced in $\sim 0.5\,\mu$m wide epitaxial cobalt dots 25 nm thick and demagnetized in the direction of the H vector. The dots were fabricated using X-ray lithography and ion–beam etching from continuous epitaxial hcp cobalt films in arrays of 5×5 mm^2. Visualization is done by a Magnetic Force Microscope (MFM). Adapted from Ref. 27.

spintronics (a neologism for spin-based electronics), the electron spin is transported from one location to another.[28] The so-called giant magnetoresistive (GMR) effect is based on the field-dependent scattering properties of electron spin. In GMR and related devices having discrete (modulated) layers, the scattering that increases the electrical resistance can be tuned.

Modulation of the structure in spintronic devices is achieved by design and manufacturing rather than as the result of a phase transition. The prototype device that is already in wide use, e.g. in most laptop computers, is a hard disk read head employing the GMR sandwich structure schematically shown in Fig. 6. This device called a spin-valve consists of thin ferromagnetic/nonmagnetic/ferromagnetic metal layers. One ferromagnetic layer has its magnetization latched by a fourth, permanently magnetic layer overlaid on it. Magnetic fringe field emanating from bits written on the hard disk change the direction of magnetization of the other, close by, ferromagnetic layer as they pass by. For ferromagnetic layers having parallel magnetization with that of the bits, the resistance to current flow is small, while antiparallel magnetization yields large resistance. At constant potential, the change in current passing through the films is sensed by an external electronic circuit to read out the bits (zeros and ones) of memory. The technology makes it possible to read out the information stored in the memory even though the physical size of a bit is very small.

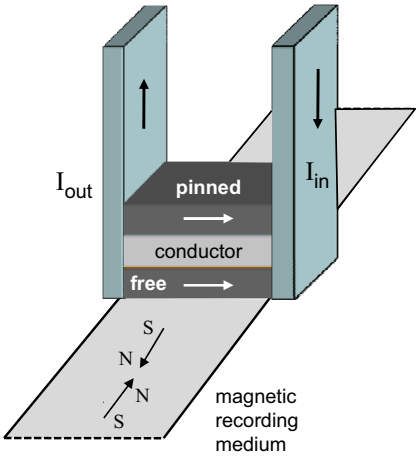

Fig. 6. A GMR magnetic media reading head. As the magnetic recording medium passes beneath the GMR sensor, it switches the direction of magnetization of the adjacent soft magnetic film. When the direction of magnetization is the same in both magnetic sensor films, the resistance to current flow is least, whereas when the directions are opposite, the resistance is greatest.

A similar structure of thin parallel layers can be configured as a magnetic tunnel junction (MTJ) for the storing of bits of information.[29] Latching of ferromagnetic films having parallel magnetization can represent a '0' while antiparallel magnetization represents a '1'. Addressing an array of the junctions is accomplished with a cross grid of normal conductors. These memory devices require no power to preserve their magnetic state and could yield computers that boot up nearly instantaneously.

7. Ferrofluids and Other Dispersions of Magnetic Particles

Much of the material of the following sections pertains to the magnetic fluids termed *ferrofluids*, suspensions of single-domain magnetic particles in a liquid carrier that are ultrastable against settling.[3] The prototypical ferrofluid is made up of magnetite (Fe_3O_4) colloidal particles having mean size (diameter) 10 nm, coated with a 2 nm monolayer of oleic acid, and suspended in a hydrocarbon carrier fluid such as kerosene. Many surfactants in addition to oleic acid are known that produce stable ferrofluids in a wide variety of liquid carriers such as other hydrocarbons, aromatics, esters, alcohols, fluorocarbon and water carriers. The particles are in rapid thermal

or Brownian motion that prevents them from settling under gravity. Concomitantly the particles collide with each other and the coating prevents the particles from agglomerating together and settling out. The particles are said to be sterically stabilized. Another class of water-based ferrofluids are ionically stabilized with electric double layers.[30]

A ferrofluid worthy of the name is free of the chaining that results from the magnetic attraction and adherence of magnetic particles to each other with an energy that exceeds that of thermal displacements. Chaining is a topic in which there is much confusion in the literature. Using the typical colloidal particle size of 10 nm and the magnetization of the usual magnetic particle magnetite, the mean number of particles in a chain computed from the deGennes and Pincus theory[31] is 1.36 in a strong H field, and 1.26 in zero field. Thus, the particles are essentially monodispersed. In simulations, the ferromagnetic particles are invariably taken to be larger and/or with stronger magnetic dipoles, resulting in particle chaining. The particle size does not have to be much larger than 10 nm before chaining becomes a practical problem in ferrofluids; at 13 nm, chains of magnetite are predicted to be infinite in length. The much larger (micrometers diameter) particles of a magnetorheological fluid (MR) chain easily, which is the basis for their applications, as discussed later.

Ferrofluids based on elemental ferromagnetic particles of iron, nickel, cobalt and their alloys oxidize after days of contact with the atmosphere and are not suitable for long–term use, except in sealed systems. But other magnetic solids such as maghemite (Fe_2O_3) and mixed metal ferrites yield ferrofluids that are long-term stable against oxidation in contact with the atmosphere.

Ferrofluids are a solution of nanometer size colloidal particles in which thermal fluctuations are a governing influence in their behavior. Accordingly, statistical mechanical analysis permits definition of the magnetization law and other physical properties. This stands in contrast, for example, to the behavior of magnetorheological fluids containing particles in the micron size range which aggregate together when subjected to applied magnetic field and require mechanical force to become redispersed. Flow of magnetic fluid in a magnetic field is subject to polarization force and constitutes a discipline in itself (ferrohydrodynamics) comparable to but distinct from magnetohydrodynamics, i.e. the flow of conductive, nonmagnetic fluid (such as molten metals) in the presence of magnetic fields. An introduction to the science with an extensive treatment of the effects of flow fields is found in the monograph of Rosensweig.[3]

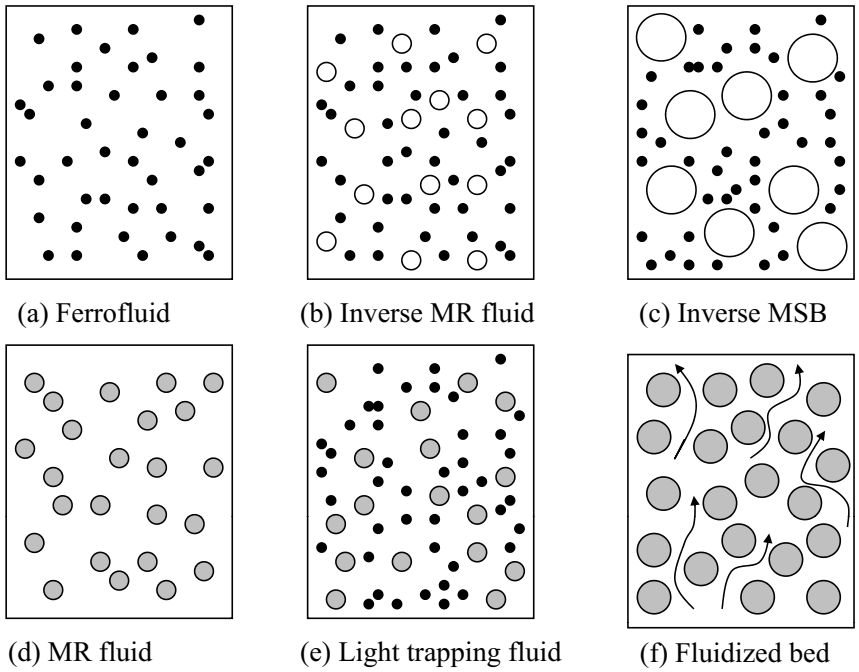

Fig. 7. Classification of particle suspensions in a fluid carrier prior to modulation by an applied magnetic field. (a) Nanometer single–domain magnetic particles in a nonmagnetic carrier; (b) Nonmagnetic micrometer size-range particles in a matrix of ferrofluid; (c) Nonmagnetic millimeter particles in ferrofluid; (d) Multi-domain magnetic particles in nonmagnetic carrier fluid; (e) Multi-domain magnetic particles in ferrofluid; (f) Multi-domain magnetic particles suspended in a flowing stream of gas or liquid. MR denotes magnetorheological. MSB denotes magnetically stabilized (fluidized) bed. Particles indicate the ordering of sizes only.

Figure 7 is a schematic illustration of six types of fluid systems containing magnetic particles that will be discussed. Four out of the six are ferrofluid systems. Black particles indicate single–domain magnetic particles having size on the order of 10 nm typical of particles in a stable ferrofluid, i.e. one which remains free of chaining of particles whether subjected to an applied magnetic field or not. Gray denotes multi-domain magnetic particles, and white denotes particles that are nonmagnetic. Modulations (e.g. formation of particle chains) can take place when the composites are subjected to an applied magnetic field. The relative sizes of the particles are not shown to scale. For example, a one micrometer particle is 10^2 times larger and a one millimeter particle is 10^5 times larger in diameter than

a 10 nm ferromagnetic particle typical of a ferrofluid. The illustrations indicate the random distribution of particles in the absence of an applied magnetic field.

7.1. *Modulation of ferrofluid interfaces*

Modulation in the physical systems discussed up to this point refer to changes in the topology of systems having essentially constant volume and overall shape. This also is the case in certain phenomena of ferrofluids; for example, phase transition in applied magnetic field. In addition, in ferrofluids an important class of modulations concerns change in the geometry of the surface or interface, as in the normal field instability and labyrinthine instability. Other modulations concern steady motions induced within the fluid itself, such as occur in field-modulated convection.

As indicated, ferrofluids exhibit a number of unique interfacial instabilities. These are phenomena occurring in ferrofluids of uniform temperature and colloidal composition. The number density of particles is on the order of 10^{23} per cubic meter, hence, the ferrofluid can be considered a continuum for most purposes. The modulations can be grouped into categories. Except where cited, the phenomena listed below are discussed in detail in Ref. 3.

- Uniform steady magnetic field applied to motionless ferrofluid
  - The normal–field instability
  - Prevention of Rayleigh–Taylor instability
  - Stabilization of a fluid column
  - Droplet shape modulation
  - Labyrinthine patterning
- Uniform steady magnetic field applied to ferrofluid in motion
  - Modulation of Kelvin-Helmholtz instability
  - Modulation of Saffman-Taylor instability
- Modulations in time-varying magnetic field[32]

Additional modulations occur in ferrofluids supporting a temperature gradient when the magnetization is temperature dependent:

- Convection of a plane layer in uniform applied magnetic field
- Convection of a plane layer in a constant magnetic field gradient

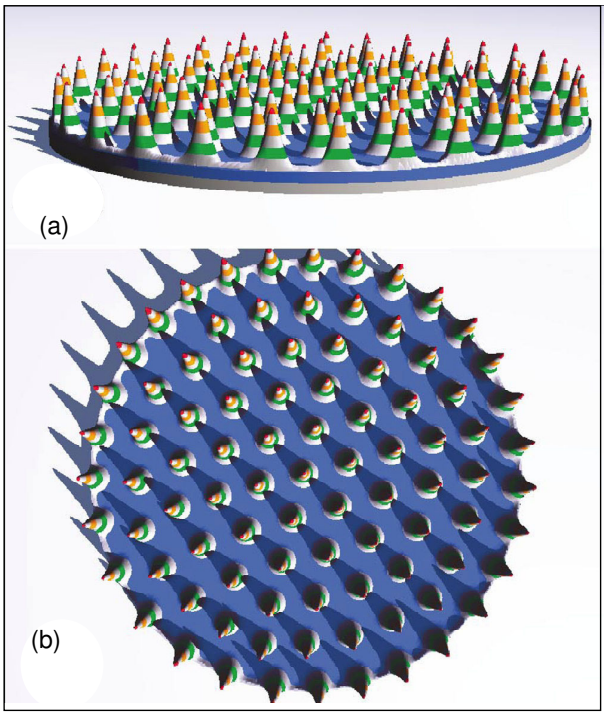

Fig. 8. Surface relief of normal-field instability of a ferrofluid reconstructed from X-ray images. (a) Oblique view. Each layer of a peak having a given color represents one millimeter of thickness; (b) Plan view. The containing vessel is 12 cm in diameter and the initial liquid depth is 3 mm. Adapted from Ref. 34.

- Convection in a spherical system with a radial magnetic field gradient[33]

The above is not an exhaustive list as systems can be rotated, concentration can be non-uniform, various instabilities can be combined, etc. In addition, in all the systems listed the magnetization is equilibrated, hence is collinear with the applied field. In comparison, in systems where the ferrofluid is subjected to rapid change in direction and magnitude of the applied field the magnetization lags the field, which excites additional forces. Modulation in this latter category is virtually unexplored.

The normal-field instability is the best known, most studied one which many refer to as the *Rosensweig instability*, see Fig. 8. Accordingly, after a brief introduction, this overview highlights a selection of related works,

many of which are concerned with non-linear aspects of this patterning phenomenon.

7.1.1. *Normal field instability*

This is the first instability of a ferrofluid to be observed; it is striking, and it is the best known. Peaks form in a patterned array on the free surface of a pool of ferrofluid when the ferrofluid is exposed to a uniform, vertically-oriented magnetic field. This pattern persists under static conditions, in contrast to patterns such as Bénard cells produced in dissipative systems far from equilibrium.

The ferrofluid pattern is sustained as a conservative system, i.e., in the absence of energy input or dissipation. The patterning can only onset in a ferrofluid having a magnetization that exceeds a critical value and was never seen until a ferrofluid having a sufficiently high magnetization was synthesized.[35] The instability in its pristine form is realized in a horizontal pool of ferrofluid subjected to a uniform, vertically oriented, magnetic field, Fig. 8. The linear analysis and experimental validation were given by Cowley and Rosensweig[36] valid for a non-linearly magnetizable fluid, where 'nonlinearly' refers to the functional dependence of magnetization on magnetic field H. The critical magnetization M_c is specified in dimensionless form by

$$\frac{\mu_0 M_c^2}{\sqrt{g\Delta\rho_m\sigma}} = 2\left(1+\frac{1}{r_p}\right) \tag{9}$$

where μ_0 denotes the permeability of vacuum, g the gravitational constant, $\Delta\rho_m$ is the difference in mass densities of fluids across the interface, σ the interfacial tension, and r_p is the dimensionless permeability ratio:

$$r_p = \left(\frac{\mu_c\mu_t}{\mu_0^2}\right)^{1/2} \tag{10}$$

For non-linear media, the parameter r_p depends on two permeabilities at the operating point: the chord permeability $\mu_c = B(H)/H$, and the tangent permeability $\mu_t = \partial B(H)/\partial H$. Although the onset of instability depends crucially on the magnetic field via the critical magnetization M_c, the spacing between peaks λ at the onset is given by

$$\lambda = 2\pi\left(\frac{\sigma}{g\Delta\rho_m}\right)^{1/2} \tag{11}$$

which is simply the capillary length between the two fluids. Note that it is the same as the wavelength at onset of Rayleigh-Taylor instability.[3]

It is instructive to indicate the physics of the normal-field instability in a simple way. Normally oriented magnetization transforms the flat surface of a pool of the ferrofluid into a lower energy surface having an array of peaks that are spaced apart from each other. The onset of the instability is governed by two conditions: i) The undulating surface has the same energy as the free surface at the point of onset; ii) Its energy is minimized at the onset.

The total energy is the sum of surface, gravitational, and magnetic terms. We will consider the energies associated with a wave train of sinusoidal form: $h(x) = \delta\cos(2\pi x/\lambda)$, where λ is the wavelength and δ is amplitude of the disturbance, assumed small.

The surface energy is proportional to the surface area. Distance along the surface between crests is given by $s \approx \lambda + (\pi\delta)^2/\lambda$. The length along the unperturbed interface is λ, hence the perturbation of surface energy is given by $\sigma(\pi\delta)^2/\lambda$, where σ is the surface tension.

The perturbation of gravitational energy along a wavelength corresponds to the work done in lifting ferrofluid from the trough region to the crest region. This is given by the product of the lifted fluid volume $\lambda\delta/\pi$ with mass density of the ferrofluid ρ_m, the distance between the centroids $\pi\delta/4$, and the gravitational acceleration g. Thus, the gravitational term is $\lambda\rho_m\delta^2 g/4$.

Rigorous formulation of the magnetic energy requires a separate computation of the magnetic field distribution to determine the energy density given by the integral of $H\mathrm{d}B$ over the system volume, before and after the perturbation of surface form. Magnetic energy density is reduced in a region occupied by the permeable ferrofluid as the fluid is more easily magnetized than empty space. Thus, because magnetization increases at the peaks of the waveform, and decreases at the troughs, the overall magnetic energy decreases with the formation of peaks and tends to offset the concomitant increase in gravitational and surface energies. At a critical value of magnetization the changes in energies balance and instability onsets.

Here we assume the energy term depends on magnetic permeability of free space μ_0, magnetization M, and wave amplitude δ. From dimensional consideration the magnetic term is thus expressed as $-\alpha\mu_0 M^2\delta^2$ where α is a proportionality factor, and the negative sign (see Sec. 3.6 of Ref. 3) corresponds to the reduction in field energy attendant to an increase of magnetization. Adding the three energy terms and factoring out δ^2 yields:

$$\sigma\pi^2/\lambda + \lambda\rho_m g/4 - \alpha\mu_0 M^2 = 0 \tag{12}$$

The equality follows from the first governing condition. Differentiation with respect to λ and rearranging yields the result of the second governing condition in the form:

$$\lambda = 2\pi\sqrt{\frac{\sigma}{g\rho_m}} \tag{13}$$

This is the expression for spacing between the peaks, the same as given by Eq. (11). Note that if λ were introduced along with or in place of δ, Eq. (13) would contain a dependence of λ on δ. This would be wrong because δ is of arbitrary size. Substituting for λ into the previous equation yields the relationship for the intensity of magnetization required for onset to occur.

$$\frac{\mu_0 M_c^2}{\sqrt{g\rho_m\sigma}} = \frac{\pi}{\alpha} \tag{14}$$

Comparison with Eq. (9) shows that $\pi/\alpha = 2(1 + r_p)/r_p$.

It is of interest to note that the onset of the normal-field instability of a ferrofluid bears analogy to the hexagonal patterns seen by direct observation in the transition of type II superconductors.[37]

In an incisive study, Gailitis[38] using an energy method to investigate nonlinear aspects of the patterning showed that the instability is subcritical, i.e. onset could occur at a lower value of applied field provided the disturbance is sufficiently large, while at the critical point the onset is 'hard', i.e. the surface deformation onsets as a jump rather than in a continuous manner. In addition, the prediction was made that the pattern, which onsets as an hexagonal array, can transform to a square array at higher applied magnetic field, and that both transitions exhibit hysteresis. Some doubt remained, however, as the analyses are restricted to small values of the relative permeability. Subsequently, however, numerical analysis[39] using the Galerkin finite element method confirmed the subcritical character of the instability and correctly predicted experimentally measured heights of the peaks, while conditions for the transition from hexagons to squares was studied by B. Abou *et al.*[40] The sketch of Fig. 9 illustrates the predictions of Gailitis.

7.1.2. *More recent work*

Interesting work has focused on the question of the shape and size of the peaks under various conditions. The most successful experimental results are obtained using the attenuation of X-rays directed vertically through

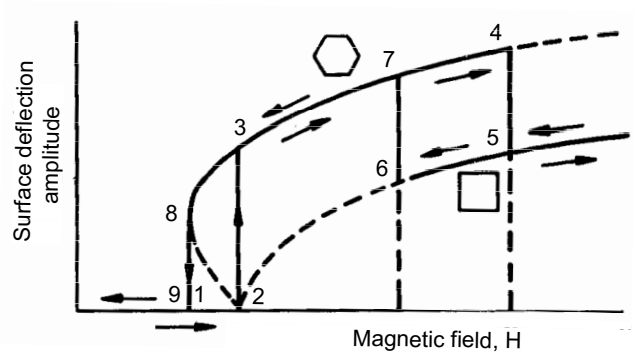

Fig. 9. Schematic illustration of transformations in the normal–field instability according to Gailitis[38] Field intensities from 1 to 2 are in the subcritical range; 2 is the onset field predicted by linear analysis; 2 to 3 represents the 'hard' transition to the hexagonal array of peaks; 4 to 5 depicts transition to a square array. Two regions of hysteresis can be seen on the curves. In decreasing field, 8 is known as the turning point. Adapted from Ref. 3.

the pool of ferrofluid.[34] In Fig. 8, which displays the usual array of peaks over the entire surface, each color indicates a layer thickness of 1 mm. This technique was applied[41] to study the surface shape generated by a local perturbation in the first subcritical hysteretic regime of the instability. This is the regime identified as 1-2-3-8-1 in Fig. 9. The perturbation is generated

Fig. 10. Nine 'solitons' (solitary structures), each generated by a transient, local pulse of magnetic field applied in the subcritical range 1-2 of Fig. 8. Peaks along rim of the container are an artifact due to the curved surface of the meniscus. The containing vessel is 12 cm in diameter and the liquid depth is 3 mm. Adapted from Ref. 41.

on a flat area of the fluid surface using a pulse of field from a small air coil placed below the center of the vessel. A single pulse produced a single peak of the hysteretic regime, and additional pulses generate additional peaks. A remarkable fact is that the peaks remain present after the pulse field is removed. The peaks are termed 'solitons' by these authors (although solitons are generally understood to refer to nonlinear traveling waves that can pass through others with no loss of form). These soliton peaks self-organize into molecule-like clusters of 2, 3, 4, 5, 6 and more peaks in symmetric arrays. Figure 10 illustrates a pattern of 9 solitons.

Figure 11 illustrates the distribution of magnetic field and cusped shape of a peak in an hexagonal array in the normal field instability as determined by a numerical computation. The concentration of field and attendant increase in normal stress difference across the interface is mainly responsible for the formation of the peaks.

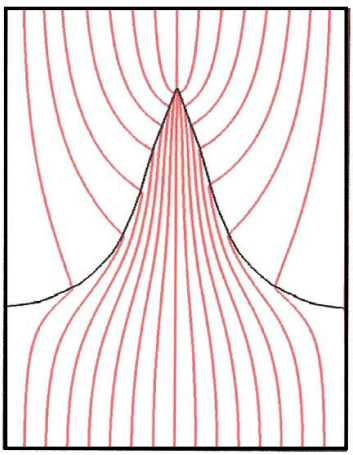

Fig. 11. Finite element computation of ferrofluid peak shape in the range 3-4 of Fig. 9 using $\mu/\mu_0 = 30$. Adapted from Ref. 42.

A simple example of parametric stabilization is the inverted pendulum whose unstable upright position can be sustained by vertically vibrating its point of suspension. In fluid dynamics a most impressive example is the inhibition of Rayleigh-Taylor instability in which a horizontal fluid layer is stabilized above another one of smaller density by vertically vibrating their container.[43] Petrelis et al[44] experimentally demonstrated the parametric

stabilization of the normal -field instability of a ferrofluid using vertical vibrations of the fluid container. The measurements were in good agreement with an analytical model.

7.1.3. *Labyrinthine instability in polarized fluids*

Labyrinthine instability of a ferrofluid shown previously in Fig. 1(c) is shown again in Fig. 12(a) alongside its dielectric dual in Fig. 12(b). The ferrofluid is contained between closely spaced horizontal glass plates (Hele-Shaw cell) together with an immiscible nonmagnetic fluid that preferentially wets the glass allowing a clear view of the pattern. A magnetic field is applied normal to the cell faces producing a pattern of stripes. The system is governed by the interaction between magnetic dipolar and interfacial energies.[4] Because thinner stripes have a fixed extent between the cell faces they possess a smaller demagnetizing field, resulting in a higher magnetization and a further reduction in magnetic energy. Concomitantly, the thinner stripes present a larger interfacial area and, hence, a larger interfacial energy which limits formation of ever thinner stripes.

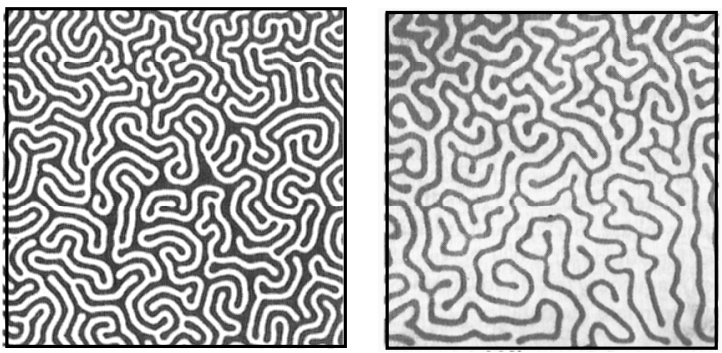

(a) Ferrofluid, $H_0 = 0.035$ tesla. (b) Dielectric fluids, $E_0 = 16$ kV/cm

Fig. 12. (a) Magnetic field applied to ferrofluid, and (b) electric field applied to dielectric oil yield labyrinthine patterning. Photos are 7 cm square. Adapted from Ref. 4.

Dielectric fluids are polarizable just as ferrofluids are magnetizable, and their response to applied electric fields provided free charge is absent is analogous mathematically and physically to the response and patterning of

the ferrofluids. Although the high intensity of the requisite applied electric field tends to be difficult to achieve, a successful implementation is shown in Fig. 12(b) using lubricating oil (dark) paired with castor oil (transparent) in a specially insulated Hele-Shaw cell. Applied electric field of frequency 500 Hz insured the absence of free charge while the insulation insured similarity of field boundary conditions at the interface between the fluids and the electrodes.

It should be noted that just as the magnetic garnet stripes in Fig. 1(a) are analogous to the ferrofluid stripes in Fig. 12(a), the stripe domains of the dipolar Langmuir monolayer shown in Fig. 3(a) are closely analogous to the dielectric labyrinth seen in Fig. 12(b). As implied previously, the magnetic systems are dual to the electric systems.

Figure 13 illustrates stages of the onset of a related phenomenon when only a small amount of ferrofluid (a drop) is put into the cell. Numerical analysis has been successful in producing realistic simulations. In one approach the dipolar energy of the system is formulated as a function of its boundary.[46] Another approach writes the free energy in terms of particle concentration expressed as a Landau expansion similar to Eq. (1), and combines these terms with a formulation expressing the surface energy.[47] The latter study predicts a further transformation of the labyrinthine pattern into a bubble array when a rotating in-plane magnetic field is superposed on the steady, perpendicular magnetic field.

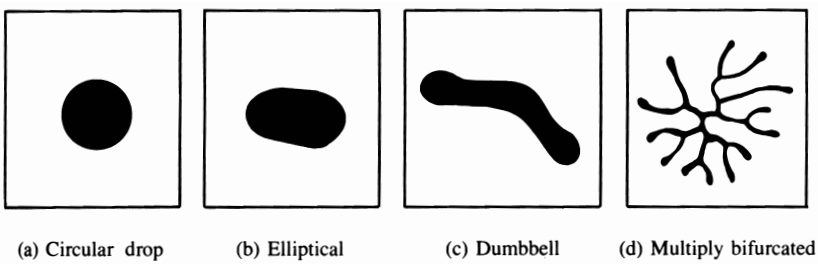

Fig. 13. Experimental transition of a circular cylindrical drop of ferrofluid in response to increasing magnetic field. Adapted from Ref. 45.

In a vertically oriented cell the two fluids form one layer over the other due to their difference in mass density, with the ferrofluid on the bottom when it is the denser. The flat interface between the fluids undergoes tran-

sition that, in addition, depends on gravitational energy.[3,35] A linearized theory predicts the onset condition[45] and the same authors present experimental photographs of the early onset terming the behavior 'comb' instability. The highly convoluted labyrinthine patterns in a vertical cell in higher applied fields are reported in Ref. 35.

Analysis using energy minimization predicts the width and spacing of stripes based on the demagnetizing field of dipoles assuming uniform magnetic surface charge on the stripe boundaries.[4] In equilibrium the net force on a whole magnetized body is given by

$$\int_V \mu_0(\mathbf{M}\cdot\nabla\mathbf{H})\,\mathrm{d}V \tag{15}$$

which transforms by vector identities to

$$\int_V \rho_{_V}\mathbf{H}_0\,\mathrm{d}V \;+\; \oint_S \rho_{_S}\mathbf{H}_0\,\mathrm{d}S \tag{16}$$

where $\rho_{_S} = \mu_0\mathbf{M}\cdot\hat{\mathbf{n}}$ is surface density of equivalent magnetic poles and $\rho_{_V} = -\mu_0\nabla\cdot\mathbf{M}$ is their volume density, $\hat{\mathbf{n}}$ is the unit normal vector facing outward from the surface.

A model stripe system is depicted in Fig. 14. Two glass plates with a spacing t in the z-direction bound an immiscible mixture of a ferrofluid and another, nonmagnetic fluid. In the model the two fluids are assumed to form a periodic pattern of infinitely long and straight stripes. The ferrofluid stripes have a width w_f in the x-direction, while the nonmagnetic ones are of width w_l. The total energy per cycle is a sum of magnetic and fluid interfacial energies, $U = U_m + U_\sigma$, where the interfacial energy $U_\sigma = 2\sigma t$ depends on the interfacial tension σ and the magnetic energy is given by

$$U_m = -\frac{1}{2}\mu_0\int_V MH_0\mathrm{d}V = -\frac{\mu_0}{2}\frac{\chi H_0^2 t w_f}{1+\chi D} \tag{17}$$

Thus, the energy per unit length along the interfacial direction is given by $U/(w_f + w_l)$.

The problem reduces to calculating the magnetization $M = \chi H = \chi H_0/(1+\chi D)$ inside the magnetic stripes of finite cross-section, where χ is susceptibility and $D = (H_0 - H)/M$ is the demagnetization coefficient. In this system with putative spatially uniform magnetization the volume density of poles disappears and only surface poles remain. The demagnetization field of the surface poles is then computed from integration of the

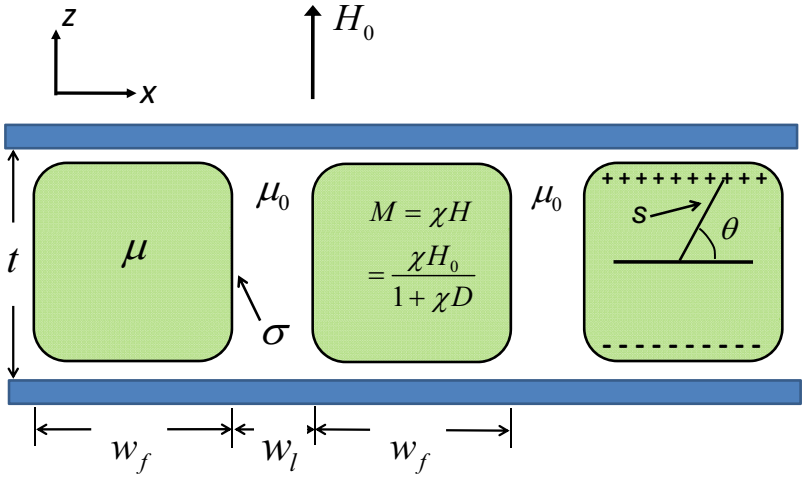

Fig. 14. The labyrinth (see Fig. 1(c)), modeled as a periodic system of infinitely long and parallel stripes in the x-direction: alternating between ferrofluid stripes with permeability μ, magnetization M and width w_f, and nonmagnetic fluid stripes of width w_l and permeability μ_0. The system has a thickness t in the z-direction which coincides with the direction of the applied field H_0. The interfacial tension between the two fluids is σ.

Coulomb expression for an infinitely long stripe, $-M \sin\theta \mathrm{d}x/2\pi s$ where $s = \sqrt{x^2 + (t/2)^2}$ is distance from the pole, x is the in-plane distance coordinate, and θ is angle subtended between s and the x coordinate (see Fig. 14).

The integration generates an infinite series of terms due to contributions from opposite poles of all the stripes. Minimization of the total energy per unit length yields the governing expression for normalized stripe width $W = w_f/t$.

$$\frac{\chi^2 N_{B_0}}{(1+\chi D)^2} \frac{\partial D}{\partial W} - \frac{2}{W^2} = 0 \tag{18}$$

and the magnetic Bond number, $N_{B_0} = \mu_0 H_0^2 t/2\sigma$ is the ratio of magnetostatic energy to interfacial energy Computation shows that stripe width decreases with increasing applied magnetic field H_0 and susceptibility χ.

The analysis above *a priori* assumes the existence of stripes and then computes their spacing. This procedure may be compared with that of sections 4 and 5, where the analysis aims at predicting both the onset and the spacing of stripe formation.

Experiments in which wall spacing and applied field were systematically varied yielded stripe thicknesses in reasonable agreement with theory over a three decade range of the magnetic Bond number. Labyrinthine patterning in dielectric fluids was demonstrated experimentally as well.[4]

For the system of Fig. 13, the superposition of an in-plane rotating magnetic field with the perpendicular time-steady normal field yields intricate and varied patterns of which some rotate. Different patterns are formed depending on which field is applied first.[32]

Finally, we note that ferrofluid in a Hele-Shaw cell exhibits a liquid froth phase similar in appearance to soap bubbles confined between closely spaced walls when subjected to oscillatory magnetic field oriented perpendicular to the layer.[48]

7.1.4. *Applications*

The normal–field instability sets a limit on certain applications where it is desired that the ferrofluid maintains a smooth surface. An illustrative example is the use of ferrofluid to produce inexpensive and versatile mirrors for astronomical optics and other uses.[49] The application has been intensely studied and found to be feasible. A reflective colloidal film of silver particles is spread on a ferrofluid and forms a mirror surface. The surface can be shaped by the application of a magnetic field to yield adaptive mirrors. Local regions of the surface can be shaped in real time by application of magnetic fields to yield adaptive mirrors that compensate for atmospheric disturbances of refractive index that, otherwise, cause 'twinkling' of stars and reduction of the resolution of images. The shape can be rapidly varied in time with surface vertical displacements ('strokes') ranging from nanometers to several millimeters. Magnetization of the ferrofluid must be kept within limits to avoid formation of peaks.

Beneficial use of peak formation is studied in a novel approach[50] to electrospinning of polymer nanofibers. A two-layered system is employed with the lower layer being a ferromagnetic suspension and the upper layer a polymer solution. Vertical peaks perturb the interfaces so that when, in addition, an electrical voltage is applied, the perturbations of the free surface are drawn out as in ordinary electrospinning. As the desired result the production rate of fiber is higher.

Electrostatic forces can be used to disrupt fluid interfaces for the production of droplets. Ferrofluid furnishes a convenient medium for the study of such electrostatic atomization as free charge is absent allowing study of the dipolar force effects in isolation.

Magnetizable elastic materials (ferrogels) can be produced when, e.g. a water–base ferrofluid is used to swell a chemically cross-linked polymer.[51] The magnetic nanoparticles attach to the flexible network of polymer chains by adhesive forces. The ferrogels can be used for switches, sensors, micromachines, biomimetric transducers, and controlled drug delivery systems that are remotely actuated with magnetic fields.[52] The normal–field instability of ferrofluids has been extended[53] to describe the deformation of these ferrogels.

7.2. *Phase transitions in ferrofluids*

A phase transition of the gas-liquid type has been observed by a number of investigators in sterically stabilized ferrofluid.[54–56] On applying an external magnetic field of critical intensity to the thin layer of the ferrofluid, highly elongated droplets of a concentrated phase of ferromagnetic colloid are formed having a clearly formed interface separating the drops from a surrounding dilute ferrofluid phase, see Fig. 15. When the applied field is removed, the elongated drops are unstable under interfacial tension and break up into smaller spherical drops that diffuse into the surroundings. The instability can also be initiated by adding a less compatible solvent to the ferrofluid. Ionically stabilized ferrofluids undergo this phase separation when electrolyte concentration is altered.[58]

Figure 16 shows the coexistence curve determined for this magnetic fluid at various dilutions. Below the curve the ferrofluid is spatially homogeneous, and above it exists the two-phase region where droplets of concentrated ferrofluid are in equilibrium with a surrounding phase of lower concentration. As previously mentioned, ionically stabilized ferrofluids can also exhibit phase separation, by applying magnetic field or, see Fig. 17, by changing the electrolyte concentration.

A thermodynamic analysis of Cebers derives the free energy of a magnetic fluid per particle, f_p, for sterically stabilized ferrofluids in the following form:[59]

$$f_p = f_0 + k_B T \ln \frac{n v_0}{1 - n v_0} - k_B T \ln \left(\frac{\sinh \xi}{\xi} \right) + \frac{1}{2} n m^2 \lambda L^2(\xi) \qquad (19)$$

where f_0 is a constant of integration, $k_B T$ is the thermal energy, n the number density of magnetic particles, v_0 the coated volume of a particle, and $\lambda = 1/3$ is the Lorentz cavity constant. The Langevin function is

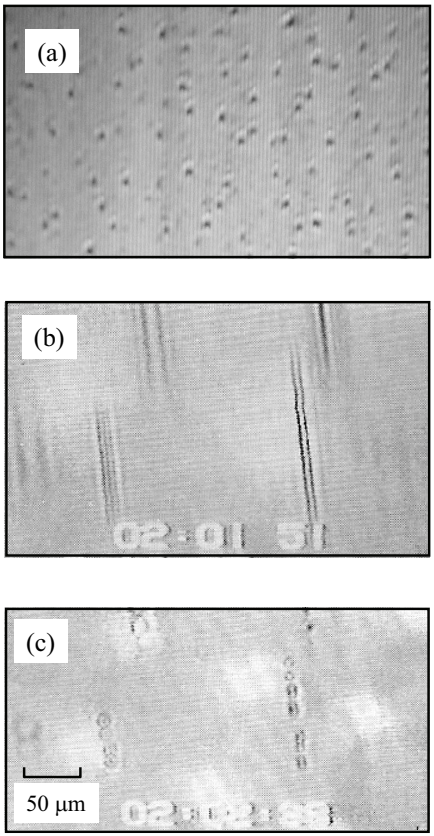

Fig. 15. (a) Droplets in a thin layer with field oriented normal to the layer of a kerosene-based sterically stabilized ferrofluid. (b) Elongated droplets induced by a $12.7\,\mathrm{kA\,m^{-1}}$ magnetic field oriented tangential to the layer. (c) Breakup into spherical droplets $\sim$0.8 s after removal of the field permits estimation of interfacial tension $\sim 8.1 \times 10^{-4}\,\mathrm{mN\,m^{-1}}$ based on viscous dominated instability as in Ref. 57; the droplets subsequently diffuse into the surrounding continuous phase. Part (b) and (c) are adapted from Ref. 56. Part (a) not previously published, is taken from a video recording.

defined as $L(\xi) = \coth(\xi) - \xi^{-1}$ and depends on a dimensionless variable ξ

$$\xi = \frac{mH}{k_B T} \tag{20}$$

$m = \mu_0 v M_d$ is the magnetic moment of a particle, where v is the volume of the magnetic core of a particle, M_d the domain magnetization, and H is the applied external field. The chemical potential per particle is obtained

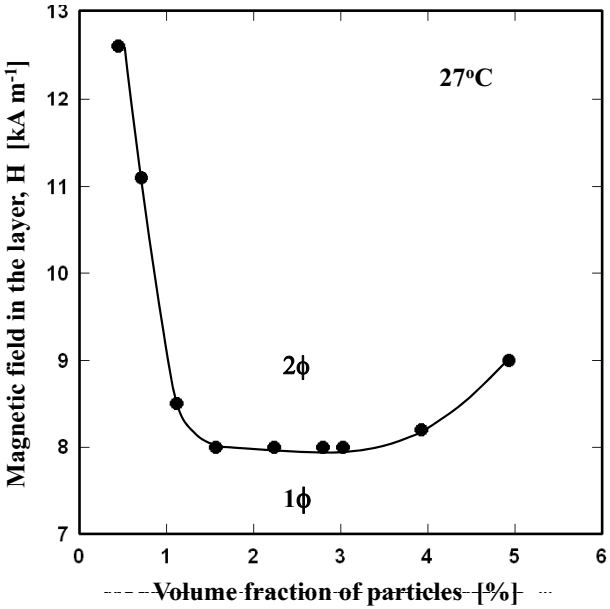

Fig. 16. Experimental spinodal data for a kerosene–based sterically–stabilized ferrofluid having mean particle size 7.4 nm. Adapted from Ref. 56.

from the free energy per unit volume nf_p:

$$\mu = \left.\frac{\partial n f_p}{\partial n}\right|_{T,H} \tag{21}$$

Prediction is made of the spinodal and binodal curves on a plot of magnetic field versus concentration. The binodal curve defines the coexistence curves and corresponds to a pair of points having a common tangent on a line osculating the free-energy curve

$$\mu(n_1, T, H) = \mu(n_2, T, H) \tag{22}$$

$$n_1[f_p(n_1, T, H) - \mu] = n_2[f_p(n_2, T, H) - \mu] \tag{23}$$

The spinodal curve corresponds to a pair of inflection points of the free energy where

$$\left(\frac{\partial \mu}{\partial n}\right)_{H,T} = 0 \tag{24}$$

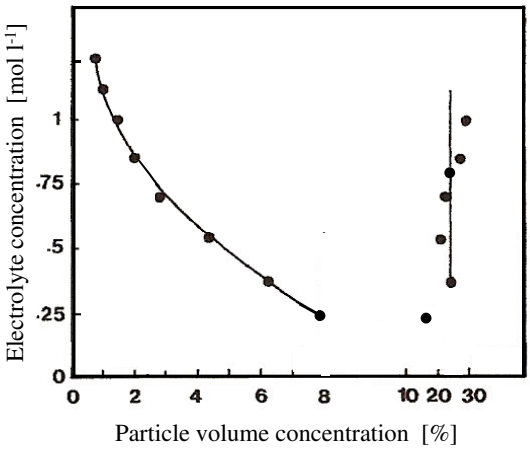

Fig. 17. Experimental phase diagram of an ionic ferrofluid. The initial uniform volume fraction of the particles is 8%. Note the change in horizontal scale at high values. Adapted from Ref. 58.

Subscripts 1 and 2 denote the dilute and concentrated coexisting phases, respectively. In the zone between the spinodal and the binodal curves the ferrofluid is metastable.

Some of the theoretical coexistence curves of the Cebers theory are qualitatively similar to the experimental curve of Fig. 16. That is, the coexistence curves are concave upward and above the curves the homogeneous solution separates into a concentrated and a dilute phase. At higher values of the ratio of particle-particle interaction to thermal-energy, phase separation at zero applied field is predicted. The theory also predicts that the concentrated phase is spontaneously magnetized in the absence of an external H field, though this is thought to be an extraneous prediction due to the use of mean-field theory. Thus, the effective field H_e acting to magnetize a particle of the ferrofluid is specified as the Lorentz relationship $H_e = H + M/3$ where H is the Maxwell field in the medium. A simple example shows the peril of this mean-field assumption. Assuming a linear medium, defining effective susceptibility $\chi_e = M/H_e$, usual susceptibility $\chi = M/H$, and solving for χ yields

$$\chi = \frac{3\chi_e}{3 - \chi_e} \tag{25}$$

This relationship predicts spontaneous magnetization when χ=3 but the behavior is not seen experimentally. The lattice-gas model of Sano and

Doi[60] yields coexistence curves that are qualitatively the same as those of the thermodynamic treatment of Cebers. The van der Waals interaction is specified as a constant value at particle contact. Interestingly, the Lorentz field condition is an outcome of the model, and not an initial assumption. A more recent treatment[61] using two models for the fluid entropy yields similar results to those of Cebers,[59] and Sano and Doi.[60]

Two other models predict an enhancement of field-induced magnetization but are free of spontaneous magnetization. One is based on the mean–spherical approximation,[62] while the other uses a perturbation treatment.[63]

A recent Monte-Carlo treatment explicitly produces the phase diagram of a ferrofluid,[64] see Fig. 18. The authors concluded that dipole-dipole and steric interactions alone can induce phase separation, and that additional attractive potentials need not be introduced.

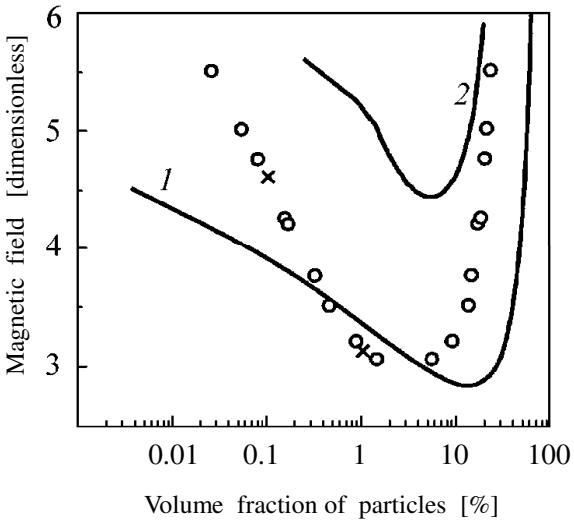

Fig. 18. Calculated phase diagram of a ferrofluid. (1) Perturbation theory from Ref. 63; (2) Mean–spherical model from Ref. 62; The symbols (o) and (x) are from Monte–Carlo simulations of Ref. 64.

We would like to return to the issue of chaining of ferromagnetic particles that was discussed in the beginning of Sec. 7. Chaining of monodisperse magnetite particles in a 2D film is evident in the experimental images of Klokkenburg *et al.*[65] obtained by cryogenic transmission electron microscopy. However, the particles have magnetic cores of 16 nm in one

sample and 20 nm in another, hence will strongly chain under the deGennes and Pincus theory.[31] The long chains have little thermal motion and hence sediment readily, especially in a strong magnetic gradient field, thus are not useful in ferrofluids.

In another work, Tlusty and Safran[66] treated phase separation of suspended dipolar particles in terms of the energy and entropy of chain free-ends and topological defects, yielding chain branching rather than the two-particle interactions of the aforementioned models. Their analysis is restricted to absence of an applied magnetic field and suggests that one phase consists of branched chains and the other of free chains. A zero-field phase-separated ferrofluid can be produced by adding a poor solvent. Such a preparation is used in Ref. 67 of Zhu *et al.*

In conclusion, the importance of these studies, aside from their inherent interest, extends possibly to the understanding of the interactions of dipolar molecules. Such species include, for example, molecules such as hydrogen fluoride and even water.

7.3. *Modulation of embedded objects*

Modulation of embedded objects in a ferrofluid has multiple interests: as a model for two dimensional melting of solids; for producing periodic structures of large molecules for analysis by scattering of waves; for self-organized manufacturing of microscopic arrays, etc.

To a first approximation, when a spherical nonmagnetic particle is dispersed in a magnetized ferrofluid the void produced by the particle possesses an effective magnetic moment, m, equal in size but opposite in direction to the magnetic moment of the displaced fluid, i.e. $m = -\mu_0 V \chi H$ where V is volume of the sphere, χ is the effective volume susceptibility of the ferrofluid, and H is the magnetic field. For relatively low fields ($\mu_0 H < 0.01\,\text{Tesla}$), χ is approximately constant and m increases linearly with H. The interaction energy between two spheres with a center-to-center separation distance r_d is given by the dipolar relationship

$$U = \frac{m^2(1 - 3\cos^2\theta)}{4\pi\mu_0 r_d^3} \tag{26}$$

θ is the angle between the line connecting the centers of the spheres and the direction of the field. A thermodynamic system is obtained by using sufficiently small spheres (of diameter $d < 2\,\mu\text{m}$) having Brownian motion. The controlling parameter determining structural modulation is the ratio between the dipolar energy and the thermal energy. From Eq. (26), using

the magnitude of U with $\theta = 0$, $r_d = d$, and ignoring a constant factor

$$\frac{\text{Dipolar energy}}{\text{Thermal energy}} = \frac{m^2/\mu_0 d^3}{k_B T} \tag{27}$$

7.3.1. *Phase change model and alignment of particles*

A monolayer of equal size nonmagnetic spheres immersed in a thin layer of magnetic fluid yields an intriguing model exhibiting phase change properties of melting.[68] This analog model utilizes micrometer-size polystyrene spheres that exhibit Brownian motion and can be viewed under a microscope as depicted in Fig. 19(a). Figure 19(b) shows that crystalline ordering of the spheres results from the application of a magnetic field oriented perpendicular to the layer. Each sphere is a hole in the magnetic fluid and acts as a magnetic dipole of reverse polarity repelled from its neighbors. Varying the field in this system changes the value of m and, hence, that of the ratio in Eq. (27), and can be considered as an adjustment of temperature in a molecular system. Thus, for example, melting or return to randomness is observed if the field is reduced. The system has been suggested for testing theories of two-dimensional melting via the vortex unbinding mechanism.[20] Shown in Fig. 19(c) is the chain formation that results from a tangential orientation of the field. In this configuration the spheres attract each other.

Ordering of dilute suspensions of macromolecules is attainable in magnetized ferrofluids for assemblies that are not amenable to conventional alignment techniques. Using this technique to obtain neutron-diffraction patterns permits study of the internal structure of macromolecules such as the tobacco mosaic virus (TMV) and tobacco rattle virus (TRV).[69] TMV is a hollow cylindrical assembly of length 300 nm, external diameter 18 nm, and internal diameter 4 nm. Similarly, TRV is 23 nm in diameter, 5 nm in internal diameter, and shorter than TRV. TMV and TRV both align when dispersed in a ferrofluid and subjected to a modest level of magnetic field. The ability of the method to work with low concentrations makes the method of particular interest for aligning biological materials such as chromatin which are not easily obtainable in quantity.

7.3.2. *Normal and inverse magnetorheological fluids*

Magnetorheological (MR) fluids are suspensions of magnetizable particles typically in the size range 2 to 10 μm in a nonmagnetic oil matrix, refer to Fig. 7(b) and (d). The particles are multi-domain and only produce a

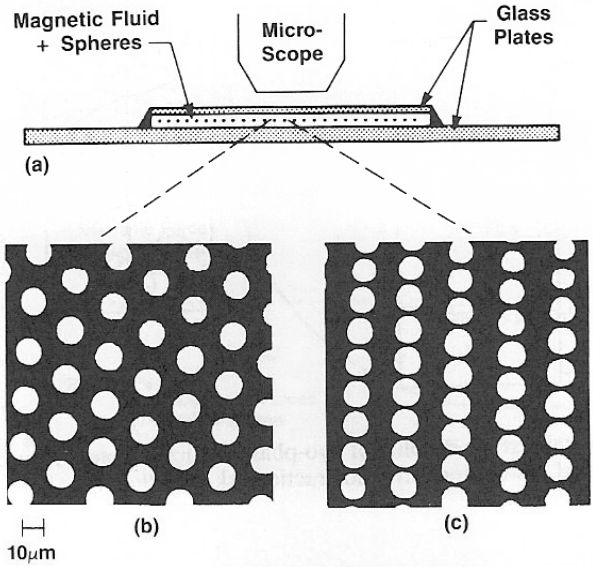

Fig. 19. (a) A side view of a single layer of nonmagnetic, micrometer-size spheres immersed in ferrofluid. (b) The layer organizes into a hexagonal lattice when field is oriented normal to the layer, and (c) into chains when field is tangential to the layer. A uniform volumetric magnetization is equivalent to a distribution of poles on the surface of the spheres. These poles confer strong diamagnetic character to the spheres. Adapted from Ref. 68.

net magnetization when a magnetizing field is applied. When subjected to a magnetic field the particles form chains resulting in the appearance of a yield stress and a large increase in viscosity. The technology dates back to the 1940s[70] with a surge of scientific interest in the 1990s due to the availability of inexpensive computer control of applied field in real time, and significant commercialization has been realized in damping of vehicle shock absorbers,[71] and production of complex optical surfaces, and other grinding and polishing applications.[72]

The suspension of nonmagnetic particles of 2 to 10 micrometer size in a matrix of ferrofluid yields an inverse magnetorheological fluid (IMR) having properties of yield stress and controllable increase of viscosity.[73] Due to the absence of particle-particle contact-magnetization that is present in ordinary MR fluids the dependence of yield stress on particle concentration in an IMR predicted from a model of asymmetric stress shows good agreement compared to data.[74]

Interest in magneto-optical effects in inverse MR fluids is found in Ref. 75.

7.3.3. *Magnetic trapping of light*

This section deals with the system shown in Fig. 7(e), a suspension of MR particles in ferrofluid as the carrier. Mehta and co-workers[76] observed that upon application of an external magnetic field on a dispersion of micrometer-sized magnetic spheres stably dispersed in ferrofluid, through which monochromatic, coherent light was passing, the light gets trapped inside the suspension for critical values of applied field. The photons remain trapped while the external magnetic field is acting. When the field is removed, photons are emitted from the medium with the same frequency as the incident light, but with lower intensity.

As long ago as 1958, trapping of light or 'localization' was predicted in strongly scattering disordered media.[77,78] The prediction received experimental confirmation first in the microwave and then in the visible using either disordered media or partially ordered structures such as liquid crystals. An interesting and potentially useful aspect of the new work is that one can tune the dielectric contrast of the micrometer-size carriers with respect to the ferrofluid by varying the applied magnetic field. A complex phenomenon is observed when the light beam is first switched off, and then with a delay, the applied magnetic field is switched off. After a total time delay of a second and a half, a flash of light appears both in the forward and backward directions,[79] see Fig. 20. This is spectacularly long compared to nanosecond delays achieved in other materials. The simplicity of the phenomenon is of interest in photonics in optical memories, small threshold micro-lasers, fast optical switches, optical transistors, and other components that many believe will supercede conventional electronics.

It is known that the micrometer-sized magnetic spheres form elongated chain-like structures under the influence of the external magnetic field, a true spatially modulated phase. The micrometer-size particles scatter light by the Mie mechanism, and the (much smaller) ferrofluid particles are Rayleigh scatterers.[80] That is, Mie theory applies to the scattering of electromagnetic radiation by particles that are similar or larger than the wavelength of light, while Rayleigh scattering applies to particles that are much smaller than the wavelength of light. It is surmised that cavities are formed within the medium in which the light is trapped. When the field is removed the chains break up, somehow releasing the light.

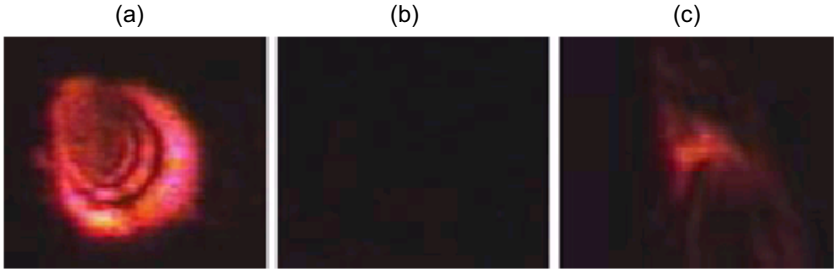

Fig. 20. (a) Diffraction pattern of red light passes through the fluid with no external magnetic field applied. (b) The pattern is stopped by a particular magnetic field strength. (c) Photons appear again when the magnet is switched off. Adapted from Ref. 76.

This phenomenon is very surprising as even the best fiber optics dissipate transmitted light in time periods on the order of a millisecond, and the particle suspension is expected to be more lossy. The phenomenon has not been independently verified yet, its mechanism is uncertain and no theory or model has appeared in the literature. Hence its status is provisional.

7.3.4. *Modulation of a nanoparticle cloud*

The micrometer–size metallic particles of an MR fluid tend to settle under gravity. The settling can be alleviated with the addition of an additive to form a gel network that is strong enough to suspend the particles, yet easy enough to yield to an applied shear stress. Another means has been reported based on a bimodal suspension of 2 μm iron particles in a matrix of magnetite ferrofluid having particles in the usual nanometer size range.[81] This is another illustration of the morphology shown in Fig. 7(e). The mechanism preventing the sedimentation appears to be related to the presence of a diffuse cloud of the magnetite particles surrounding each particle of iron, see Fig. 21. Presumably the cloud forms because of dipole-dipole magnetic attraction due either to remanent or induced dipoles of the iron particles and their interaction with the permanent dipole moments of the ferrofluid particles.

A model of nanoparticle cloud distribution under the influence of van der Waals forces treated as a variational problem is found in Ref. 82, and the same methodology should be useful in treating the magnetic problem. The model also predicts a repulsion between the larger particles when their associated clouds overlap, a mechanism that would help to alleviate sedimentation.

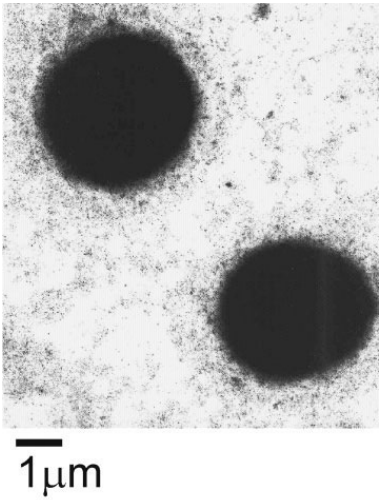

Fig. 21. Transmission electron microscopy of bimodal particle mixture showing a diffuse cloud of magnetite nanoparticles surrounding micrometer–size iron particles. Adapted from Ref. 81.

7.3.5. *Magnetically stabilized fluidized bed (MSB)*

This section concerns particulate systems of the type depicted in Fig. 7(f).

Gas fluidized beds of particulates are industrially important as are liquid fluidized beds. In nature, quicksand is an example of the latter. When the particles are magnetizable and a magnetic field is applied, new modulational behavior arises, as will be discussed. If system conditions produce strong chaining, the desirable features of the MSBs can be lost and so must be avoided. Thus, the study of chaining can be valuable for defining the useful limits of operation. That useful MSBs are free of chaining is documented in a study[83] wherein the bed was encased in polymer, sections taken and polished, and examined under a microscope.

As the velocity of a gas flowing upward through a bed of particles is increased [see Fig. 7(f)], a point is reached where the bed becomes unweighted and is said to be fluidized. Any excess gas collects into bubbles having a sharp interface that are buoyant and rise, stirring the contents of the bed and back mixing the solids. These fluidized beds have industrial importance in processing petroleum vapors and chemicals where it is desired to achieve good contacting of vapors with solids while the back mixing maintains a constant temperature throughout. In other applications it would be

desirable to prevent the formation of the bubbles, e.g. to create a moving bed contactor with continuous input and output of the solids.[84]

A stability analysis treating the bed as a continuum and determining the time evolution of a voidage wave passing through shows that if the particles are magnetizable and a uniform magnetic field applied, the formation of the bubbles can be totally prevented over a wide range of flow rates.[85] The prediction is well confirmed by laboratory tests. Flow rates in excess of minimum fluidization velocity expand the bed. Here the boundary between stably and unstably fluidized regimes is similar to a coexistence curve. The operating regimes of the bed are depicted in the diagram of Fig. 22, which mirrors the appearance of a phase diagram of a molecular system. However, in this case the particles are typically in the sub-millimeter to millimeter size range and Brownian motion is negligible.

An inverse composite, refer to Fig. 7(c), using one millimeter, hollow glass spheres, fluidized by upflow of a ferrofluid also exhibits magnetic

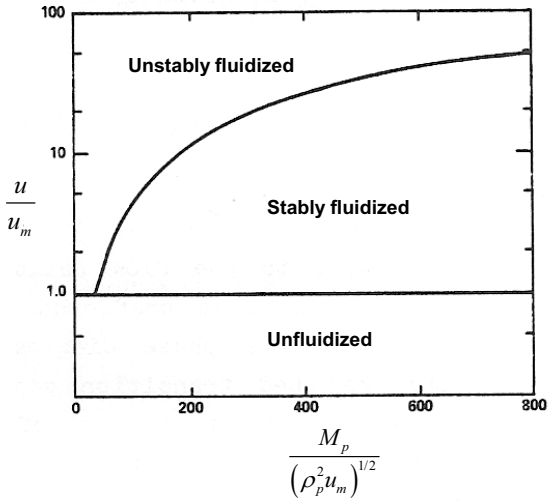

Fig. 22. Predicted phase diagram of a magnetically stabilized fluidized bed (MSB). The unfluidized regime is the analog of the solid state, stably fluidized the liquid state, and unstably fluidized the gaseous state. Thus, velocity plays the role of temperature, and magnetization the role of pressure. In the stably fluidized state an object less dense than the expanded bed floats, and surface waves can propagate across the free interface at the top of the bed. u denotes superficial velocity, u_m minimum fluidization velocity, M_p particle magnetization, and ρ_p particle mass density. M_p is a function of the applied, modulating field H; when the field is removed $M_p = 0$ and the stably fluidized regime disappears. Adapted from Ref. 86.

stabilization in an applied magnetic field. As a variant of the magnetically stabilized fluidized bed (MSB), the stabilization also prevents bed instability that usually results in back mixing, bypassing of the fluidizing fluid and chaotic flow.[87] Quantitative agreement of the experimental coexistence curve with the theory is close compared to that for the ordinary MSB.[87] This is believed due to the strong local polarization that occurs at the contact region of a pair of highly permeable magnetic particles. The resultant attractive force between such particles confers a Bingham-type rheology to the bed which is not modeled in the theory. This complication is absent in the inverse beds.

7.3.6. *Other related phenomena*

A number of other multiphase ferrofluid systems are reviewed by Cabuil and Neveu.[88] These include magnetic lamellar phases consisting of a periodic packing of alternate water and ferrofluid layers, mixture of ferrofluid with liquid crystalline carrier, magnetic vesicles, and magnetic emulsions. Modulating the alignment of a nematic liquid crystal by doping it with a small amount of ferrofluid, in principle, can be accomplished using just a weak magnetic field on the order of 10^{-2} tesla as was first suggested in the classic paper of Brochard and de Gennes.[89] Recent work explores the synthesis of ferrofluids amenable to the doping.[90]

Ferroelectric analogs to ferrofluids conceptually employ a particle such as barium titanate that is permanently electrically polarized, and would respond to electric fields in the manner that ferrofluids respond to magnetic fields. However, attempt to produce such a dispersion have been unsuccessful. It is thought that the association of free charge neutralizes the polarity of the dispersed particles, a process that cannot occur in ferrofluids as magnetic monopoles are not found in nature. In contrast, there is much interest for technological applications of electrorheological (ER) fluids.[91] In these systems larger particles are dispersed in a good insulator fluid. The polarization is not inherent to the particles but is induced by an external electric field and arises from the substantial dielectric difference between the particles and the carrier fluid.

8. Block Co-Polymers

For our last example, we depart from magnetic colloids and granular magnetic systems to review the appearance of modulated phases in block

copolymers (BCP). These are polymeric systems in which each polymer chain is composed of several homogeneous blocks. Block copolymers exhibit a fascinating variety of self-assembled nanoscale structures with various types of chain organization. We focus only on the simplest, linear A-B di-block chain architecture, in which a homogeneous and long polymer chain of type A is covalently bonded with a B chain.[13,14,92–95] Composite materials made by mixing two or more different types of polymers are often incompatible and undergo phase separation. Such macrophase separation is hindered in BCP systems due to the chain connectivity.

By properly choosing the polymer blocks, it is possible to design novel composite materials made of BCP chains with desired mechanical, optical, electrical and thermodynamical properties.[13] For example, by joining together a stiff (rod-like) block with a flexible (coil) block, one can obtain a material that is rigid, but not brittle. Moreover, the interplay between flexibility and toughness can be controlled by temperature. More recently, BCPs are being explored in applications such as photonic band–gap materials, dielectric mirrors, templates for nano-fabrications and in other optoelectronic devices.[96,97]

Liquid melts of block copolymers or BCP-solvent liquid mixtures form spatially modulated phases in some temperature range. As an example we show in Fig. 23 the multitude of modulated phase in the well-studied polystyrene–polyisoprene (PS-PI) block copolymer system.[98] The two important parameters that determine the phase diagram of the figure are the mole fraction of one of the two components, f_A, and the product of two parameters, $N\chi_{\rm AB}$, where $N = N_A + N_B$ is the BCP chain degree of polymerization (total number of monomers), and $\chi_{\rm AB} \sim T^{-1}$ is the Flory constant. The latter is a dimensionless parameter representing the ratio between the interaction energy to the thermal energy k_BT, and quantifies the relative interaction between the A and B monomers. Typical values of $\chi_{\rm AB}$ are small compare to unity (about $\chi_{\rm AB} \simeq 0.1$ for styrene-isoprene).

At high temperatures (low value of $N\chi_{\rm AB}$) the BCP melt is in a disordered liquid state in which the different chains show no particular organization. As the temperature is reduced below some critical value ($N\chi_c \approx 10.5$ in Fig. 23), the partially incompatibility between the A and B blocks causes a micro-phase separation into one of several modulated phases. These so-called meso-phases have spatial modulation in the 10 — 100 nm range and can have several symmetries. Figure 23 shows the lamellar (LAM), hexagonal (HEX), body centered cubic (of group symmetry $\mathrm{Im}\bar{3}\mathrm{m}$) and bicontinuous gyroid (of group symmetry $\mathrm{Ia}\bar{3}\mathrm{d}$) phases, as well as a perforated

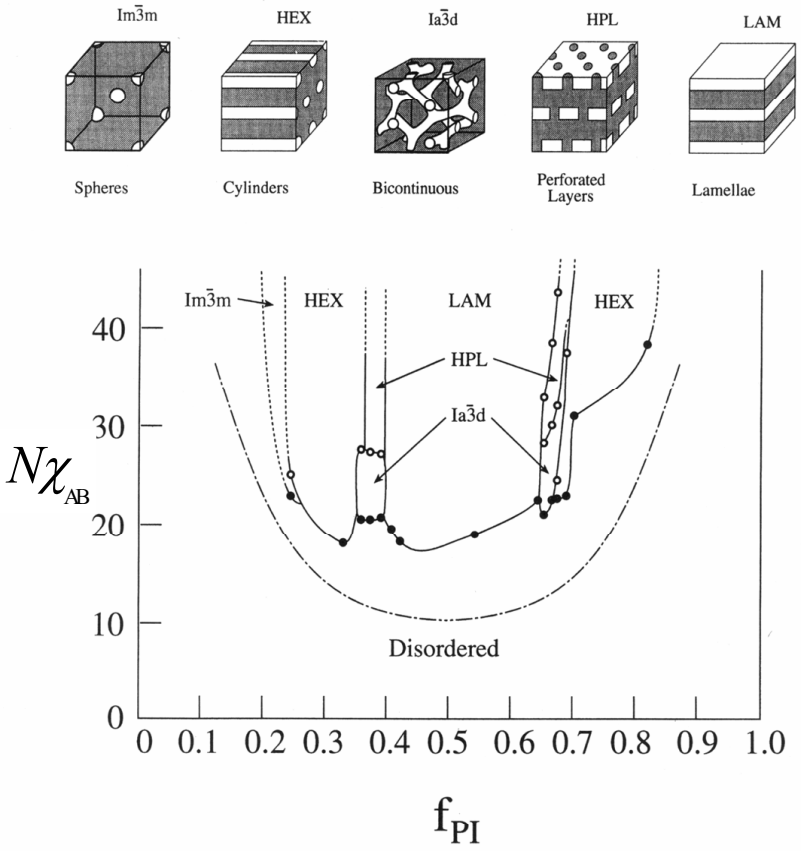

Fig. 23. $N\chi_{AB}$ versus f_{PI} phase diagram for PI-PS di-block copolymers, where f_{PI} is the mole fraction of the isoprene block. The dash-dot curve is the mean-field prediction for the instability of the disordered phase. Solid curves are experimental ones and have been drawn to delineate the different phases observed but might not correspond to precise phase boundaries. Five different ordered microstructures (shown schematically) have been observed for this chemical system. Adapted from Ref. 98.

lamellar phase (HPL) that is believed to be a long-lived metastable state, but not a true, thermodynamic stable phase.

8.1. *Modulated periodicity in BCP*

How can we understand the self-assembly and stability of various BCP modulated phases with definite periodicity? While sophisticated theories[93,99–106] quite successfully reproduce complex phase diagrams such as

Fig. 23, we present here a qualitative and heuristic explanation.[92] Consider a symmetric di-block copolymer ($f_A = N_A/N = 0.5$) whose structure is that of a lamellar stack as depicted in Fig. 24. The uni-directional periodicity d is taken as parameter and its value will be determined later. We also assume that the two blocks have the same monomer size, a. If the A and B chains were not connected, the coarsening that usually occurs during phase separation would result in a macro-phase separation (theoretically with $d \to \infty$). However, as the BCP periodicity d increases, the A-B chains start to stretch and lose entropy. The competition between coarsening and chain entropy results in a preferred domain size d; this is a characteristic of all BCP systems. For a lamellar phase with $f_A = 0.5$, the free energy per copolymer chain can be written as a sum of two terms

$$f_{\text{chain}} = k_B T \frac{3(d/2)^2}{2Na^2} + \sigma\Sigma \tag{28}$$

The first term expresses the entropy cost of stretching an ideal chain (similar to a Gaussian random walk) of N monomers to span half of the lamellar period, $d/2$, from its unperturbed size $=aN^{1/2}$. The second term is the interfacial energy per chain where $\sigma \sim \chi_{\text{AB}}^{1/2}$ is the surface tension (in units of energy per area), and Σ is the area per chain at the A/B interface. Because we consider a di-block polymer melt (i.e. with no solvent), the system is assumed to be incompressible: the volume occupied by each chain is fixed,

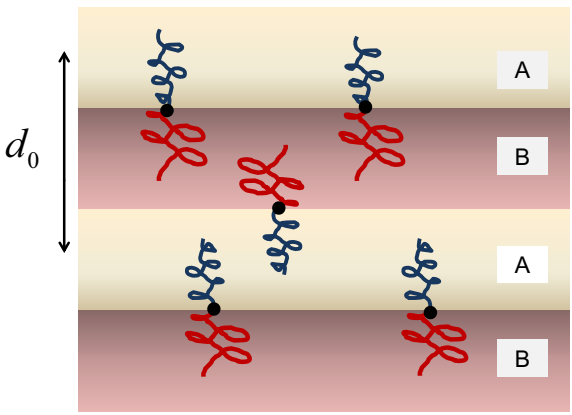

Fig. 24. Schematic representation of a symmetric lamellar phase of di-BCP ($f_A = 0.5$). The periodicity d_0 is twice the thickness of each of the A and B lamellae.

$v_{\rm chain} = Na^3 = \Sigma d/2$, where a^3 is the volume of one monomer. Substituting the incompressibility condition, $\Sigma \sim d^{-1}$, in Eq. (28), the chain free–energy is minimized with respect to the lamellar thickness d whose optimal value is

$$d_0 \simeq 1.39 \left(\frac{\gamma_{AB}\sigma a^2}{k_B T}\right)^{1/3} a N^{2/3} \sim \chi_{\rm AB}^{1/6} N^{2/3} \tag{29}$$

where we used the simple scaling dependence of σ on $\chi_{\rm AB}$. Hence, from a simple free–energy minimization we find that the lamellae have a preferred periodicity $d_0 \sim N^{2/3}$ that scales as the two-thirds power of the BCP molecular weight; this should be compared with the unperturbed size $\sim N^{1/2}$. Hence, this means that the BCP chains in a lamellar phase are highly stretched due to their partial incompatibility. The prediction of novel structures using a simple free–energy minimization subject to structural and composition constraints is an essential element behind the more refined theories[93] and is characteristic of all BCP systems.

8.2. *Orientation of anisotropic phases by an electric field*

As noted previously, block copolymers form heterogeneous composite materials. Since most polymers are non-conducting dielectrics, a modulated phase of BCP is a heterogeneous dielectric, with spatially varying dielectric constant that depends on the dielectric constants of the two blocks, ε_A and ε_B. When an anisotropic BCP phase (such as a lamellar stack or an hexagonal arrangement of cylinders) is placed in a strong enough external electric field , E, the most apparent effect is an orientation of the BCP domains in the direction of the external field.[107–117] The term in the free energy accounting for this effect is proportional to $(\varepsilon_A - \varepsilon_B)^2 E^2$. In coarse grained models of BCP melts, only the local relative A/B concentration is retained. It is represented by a continuous composition variable, $\phi(\mathbf{r})$, that varies between zero (pure B) and one (pure A). The dielectric constant can be taken as a linear interpolation of the local composition ϕ: $\varepsilon(\mathbf{r}) = \phi(\mathbf{r})\varepsilon_A + (1 - \phi(\mathbf{r}))\varepsilon_B$, and its spatial average is $\langle\varepsilon\rangle = f_A\varepsilon_A + (1-f_A)\varepsilon_B$. In the weak segregation limit ($\chi_{\rm AB} \approx \chi_c$), the electrostatic energy per unit volume was shown by Amundson and Helfand[108] to have the form

$$\frac{(\varepsilon_A - \varepsilon_B)^2}{2\langle\varepsilon\rangle} \sum_{\mathbf{q}} \frac{(\mathbf{q}\cdot\mathbf{E})^2}{q^2} \phi_{\mathbf{q}}\phi_{-\mathbf{q}} \tag{30}$$

where the sum is taken over all Fourier modes: $\phi(\mathbf{r}) = \sum_{\mathbf{q}} \phi_{\mathbf{q}} \cos(\mathbf{q} \cdot \mathbf{r})$. Minimizing the sum of the electrostatic energy Eq. (30) and the non-electrostatic BCP free energy produces an orientation transition[107] shown in Fig. 25. At large enough E field, there is a first–order transition to a lamellar phase that is oriented in the direction parallel to the E field (the y axis in the figure). The modulations seen in Fig. 25(b) are typical of the weak segregation limit and disappear for larger E fields. In other works, such electric-field orientation was also reported for cylindrical phases.[117,118]

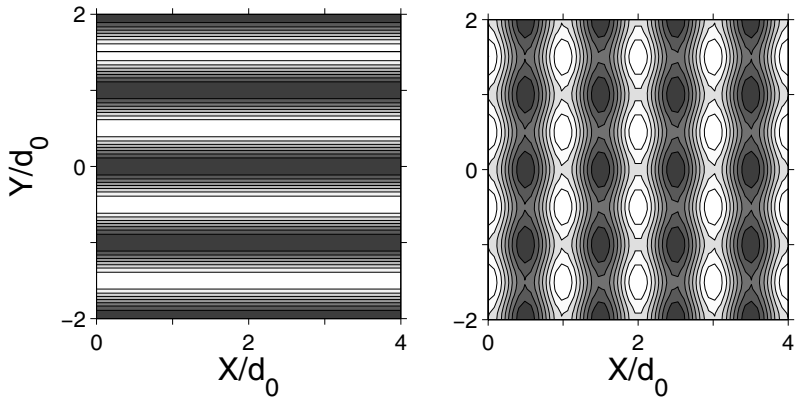

Fig. 25. Calculated contour plots of a symmetric BCP lamellar phase between two planar electrodes and under external electric field. The electrode surfaces are at $y = \pm 2d_0$, and the field is in the y direction. The B monomers (colored black) are attracted to both surfaces. (a) For E–field slightly smaller than the critical field, $E = 0.98E_c$, the film exhibits a perfect parallel ordering. (b) For E-field just above the threshold, $E = 1.02E_c$, the film morphology is a superposition of parallel and perpendicular lamellae. Adapted from Ref. 107.

8.3. *Phase transitions induced by electric fields*

It is well known that a drop of ferrofluid placed in a strong magnetic field elongates into a prolate ellipsoid and then, via a first-order phase transition, sharply transforms into a needle-like drop.[3]

This transition also occurs for charged or dipolar liquid drops. Quite recently a similar phenomenon was observed and modeled in bulk BCP systems.[119–122] The starting point is a cubic (bcc) phase of isolated spherical drops rich in one of the blocks (say A), embedded in a background of the

other component (B). As can be seen in Fig. 26, this situation occurs for asymmetric BCP ($f_A \neq 0.5$). When such a cubic phase of spheres (bcc) is placed in an external E field, each of the spheres elongates in the same (1 1 1) direction of the E field [Fig. 26 (a)]. As the value of the E field increases, above a critical value E_c, the distorted cubic phase undergoes a first-order phase transition to an hexagonal phase of cylinders pointing also along the same E-field direction, Fig. 26 (b).

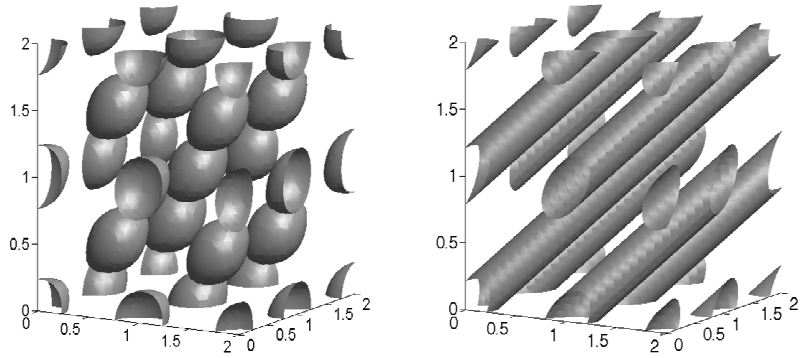

Fig. 26. Contour plots of a BCP phase in an electric field with $f_A = 0.37$ and $N\chi_{\rm AB} = 12$. At zero E field, the stable phase is a cubic phase (bcc) (not drawn). (a) For $E = 0.98E_c$, just 2% below the critical field, and oriented along the (1 1 1) direction of the lattice, each of the spheres deforms into a prolate ellipsoid and the bcc phase changes continuously into a phase with an R$\bar{3}$m space group symmetry. (c) For $E = 1.02E_c$, just 2% above the critical field, the system undergoes a first-order phase transition into an hexagonal array of cylinders, also pointing along the E–field direction. Adapted from Ref. 120.

Using two different computational techniques, the full phase diagram in the parameter space of f_A, $\chi_{\rm AB}$ and E can be calculated with semi-quantitative agreement between the two methods. The resulting phase diagram for a fixed value of $f_A = 0.3$ is shown in Fig. 27. The distorted cubic phase has an R$\bar{3}$m group symmetry, and undergoes a phase transition to an hexagonal phase (hex) or a completely disorder phase (dis) depending on the initial value of the Flory constant, $\chi_{\rm AB}$. Although the full phase diagram has not yet been measured, some of the observations agree with the model presented here for the PS-PMMA (polystyrene-polymethylmethacrylate) system.[119] We end this section by mentioning that mobile ionic impuri-

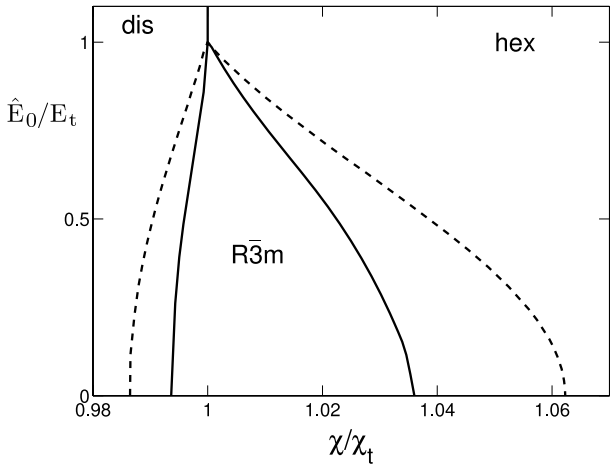

Fig. 27. Phase diagram of block copolymers in an electric field, in the plane defined by the Flory constant χ_{AB} and the normalized electric field $\hat{E}_0$, for $f_A = 0.3$. The distorted bcc phase, denoted by its space group symmetry as R$\bar{3}$m, is bounded by the hexagonal (hex) and disordered (dis) phases and terminates at a triple point where all three phases coexist. The solid line is the prediction of an analytical one-mode approximation, whereas the dashed lines are obtained by a more accurate, self-consistent numerical study. The axes are scaled by (χ_t, E_t), which are the values of χ_{AB} and $\hat{E}_0$ at the triple point. Adapted from Ref. 121.

ties can have an important effect on the phase transitions and alignment of modulated BCP phases, and is an active field of current investigations[120,123]

9. Conclusions

This review considered modulated phases in a broad context encompassing scales ranging from the nano- to the macro-scale in materials as diverse as solid state metallics, inorganics and organics. Modulations in engineering systems such as fluidized beds, magnetorheological fluids, and block copolymers are also discussed. In equilibrated systems, the structure that develops is often due to a competition between the various energies associated with the structure and yields interesting visual patterning. Many of these patterns can be understood using an energy minimization that relies on Ginzburg-Landau type free energy expansions which preserve the system symmetry or simple geometric considerations. In addition, some dissipative structures are considered as well as certain solid state devices whose structure is fabricated by pattering. The modulating methods are

complementary to each other with analysis of the dissipative structures requiring a mechanistic approach rather than an energy minimization. Some of the modulated phases are associated with significant technical applications, while others are related to biomaterials and biological systems.

Acknowledgments

We thank S. Safran for his comprehensive and incisive comments on the manuscript, and D. Ben-Yaakov, M. Schick, and Y. Tsori for additional useful comments. DA acknowledges support from the Israel Science Foundation (ISF) under grant no. 160/05 and the US-Israel Binational Foundation (BSF) under grant no. 2006055.

References

1. M. Seul and D. Andelman, Domain shapes and patterns: the phenomenology of modulated phases, *Science* **267**, 476–483 (1995).
2. M. Seul, L. R. Monar, L. O'Gorman, *Philos. Mag. B* **66**, 471 (1992); M. Seul and R. Wolfe, *Science* **254**, 1616 (1991).
3. R. E. Rosensweig, Ferrohydrodynamics (Cambridge University, New York, 1985). Reprinted with minor updates by (Dover, Mineola, NY, 1997).
4. R. E. Rosensweig, M. Zahn and R. Shumovich, Labyrinthine instability in magnetic and dielectric fluids, *J. Magn. Magn. Mater.* **39**, 127–132 (1983).
5. F. Elias, C. Flament, J.-C. Bacri and S. Neveu, Macro-organized patterns in a ferrofluid layer: Experimental studies, *J. Phys. I (France)* **7**, 711–728 (1997).
6. C. Kooy and U. Enz, *Phillips Res. Rep.* **15**, 7 (1960); J. A. Cape and G. W. Lehman, *J. Appl. Phys.* **42**, 5732 (1971).
7. T. H. O'Dell, *Rep. Prog. Phys.* **49**, 509 (1983); A. H. Eschenfelder, Magnetic bubble technology (Springer-Verlag, Berlin, 1980).
8. C. L. Dennis, R. P. Borges, L. D. Buda, U. Ebels, J. F. Gregg, M. Hehn, E. Jouguelet, K. Ounadjela, I. Petej, I. L. Prejbeanu and M. J. Thornton, The defining length scales of mesomagnetism: a review, *J. Phys.: Condens. Matter* **14**, R1175–R1262 (2002).
9. D. J. Keller, H. M. McConnell and V. T. Moy, *J. Phys. Chem.* **90**, 2311 (1986).
10. D. Andelman, F. Brochard and J.-F. Joanny, Phase transitions in Langmuir monolayers of polar molecules, *J. Chem. Phys.* **86**, 3673–3681 (1987).
11. R. P. Huebener, Magnetic flux structures in superconductors (Springer-Verlag, Berlin, 1979); T. E. Faber, *Proc. R. Soc. London Ser. A* **248**, 460 (1958).
12. E. L. Thomas and T. Witten, *Physics Today* **21**, 27 (July 1990).

13. I. W. Hamley, The physics of block copolymers (Oxford university, Oxford, 1998).
14. Y. Tsori and D. Andelman, Coarse graining in block copolymer films, *J. Polym. Sci.: Part B Polym. Phys.* **44**, 2725–2739 (2006).
15. C. Kittel, Introduction to solid state physics (J. Wiley, New-York, 2004), 8th ed.
16. P.-E. Weiss, *J. Physique Radium* **6**, 661–690 (1907).
17. L. D. Landau and E. M. Lifshitz, Phys. Z. Sowetunion **8**, 153 (1935); *Landau Collected Papers* (no. 30), D. Ter Haar, Ed. (Gordon and Beach, Ney York, 1965).
18. C. Kittel, *Rev. Mod. Phys.* **21**, 541–583 (1949).
19. A. Hubert and R. Schäfer, Magnetic domains — the analysis of magnetic microstructures (Springer, Berlin, 1998).
20. P. M. Chaikin and T. C. Lubensky, Principle of condensed matter physics (Cambridge University, New York, 2000).
21. Very close to T_c it was shown that critical fluctuations can change the nature of the transition: S. A. Brazovskii, *Sov. Phys. JETP* **41**, 85 (1975).
22. H. M. McConnell, *Annu. Rev. Phys. Chem.* **42**, 171–195 (1991)
23. G. L. Gaines, Insoluble monolayers at lipid-gas interfaces (Interscience, New York, 1966).
24. H. Möhwald, Structure and dynamics of membranes (Elsevier, Amsterdam, 1995).
25. M. F. Schneider, D. Andelman and M. Tanaka, stripes of partially fluorinated alkyl chains: Dipolar Langmuir monolayers, *J. Phys. Chem.* **122**, 094717 (2005).
26. T. Garel and S. Doniach, *Phys. Rev. B* **226**, 325 (1982).
27. M. Hehn, K. Ounadjela, J.-P. Bucher, F. Rousseaux, D. Decanini, B. Bartenlian and C. Chappert, *Science* **272**, 1782 (1996).
28. S. A. Wolf, D. D. Awschalom, R. A. Buhrman, J. M. Daughton, S. von Molnár, M. L. Roukes, A. Y. Chtchelkanova and D. M. Treger, Spintronics: A spin based electronics vision for the future, *Science* **294**, 1488–1495 (2001).
29. A. Fert, J.-M. George, H. Jaffrès, R. Mattana and P. Seneor, The new era of spintronics, *Europhys. News* **24**, No. 6 (2003).
30. R. Massart, Preparation of aqueous magnetic liquids in alkaline and acidic media, *IEEE Trans. Magnetics* **MAG-17**(2), 1247–1248 (1981).
31. P. G. deGennes and P. A. Pincus, Pair correlations in a ferromagnetic colloid, *Phys. Kondens. Mat.* **11**, 189 (1970).
32. S. Rhodes, J. Perez, S. Elborai, S.-H. Lee and M. Zahn, Ferrofluid spiral formations and continuous-to-discrete phase transitions under simultaneously applied DC axial and AC in-plane rotating magnetic fields, *J. Magn. Magn. Mater.* **289**, 353–355 (2005).
33. R. E. Rosensweig, J. Browaeys, J.-C. Bacri, A. Zebib and R. Perzinski, Laboratory study of spherical convection in simulated central gravity, *Phys. Rev. Lett.* **83**, 4904–4907 (1999).

34. R. Richter and J. Blasing, Measuring surface deformations in magnetic fluid by radioscopy, *Rev. Sci. Instr.* **72**, 1729–1733 (2001).
35. R. E. Rosensweig, Magnetic fluids, *Sci. Am.* **247**, 136–145 (1982).
36. M. D. Cowley and R. E, Rosensweig, The interfacial stability of a ferromagnetic fluid, *J. Fluid Mech.* **30**, 671–688 (1967).
37. U. Essmann and H. Trauble, The direct observation of individual flux lines in type II superconductors, *Phys. Lett. A* **24**, 526–527 (1967).
38. A. Gailitis, Form of surface stability of a ferromagnetic fluid, *Magnetohydrodynamics* **5**, 44–45 (1969); see also, A. Gailitis, Formation of the hexagonal pattern on the surface of a ferromagnetic fluid in an applied magnetic field, *J. Fluid Mech.* **82**, 401–413 (1977)
39. A. G. Boudouvis, J. L. Puchalla, L. E. Scriven and R. E. Rosensweig, Normal field instability and patterns in pools of ferrofluid, *J. Magn. Magn. Mater.* **65**, 307–310 (1987).
40. B. Abou, J.-E. Wesfreid and J. Roux, The normal–field instability in ferrofluids: hexagon-square transition mechanisms and wavenumber selection, *J. Fluid Mech.* **416**, 217–237 (2000).
41. R. Richter and I. V. Barashenkov, Two-dimensional solitons on the surface of magnetic fluids, *Phys. Rev. Lett.* **94**, 184503.1–4 (2005).
42. A. Boudouvis, private communication (2007).
43. G. H. Wolf, Dynamic stabilization of the interchange instability of a liquid-gas interface, *Phys. Rev. Lett.* **24**, 444–446 (1970).
44. F. Petrelis, E. Falcon and S. Fauve, Parametric stabilization of the Rosensweig instability, *Eur. Phys. J. B* **15**, 3–6 (2000).
45. A. O. Tsebers and M. M. Maiorov, Magnetostatic instabilities in-plane layers of magnetizable liquids, *Magnetohydrodynamics* **16**, 21–28 (1980).
46. D. P. Jackson, R. E. Goldstein and A. O. Cebers, Hydrodynamics of fingering instabilities in dipolar fluids, *Phys. Rev. E* **50**, 298–307 (1994).
47. A. Cebers, Dynamics of the labyrinthine patterns at the diffuse phase boundaries, *Brazilian J. Phys.* **31**, 441–445 (2001).
48. F. Elias, C. Flament, J.-C. Bacri, O. Cardoso and F. Graner, Two-dimensional magnetic liquid froth: Coarsening and topological correlations, *Phys. Rev. E* **56**, 3310–3318 (1997).
49. E. F. Borra, A. M. Ritcey, R. Bergamasco, P. Laird, J. Gringras, M. Dallaire, L. Da Silva and H. Yockell-Lelievre, Nanoengineered astronomical optics, *Astronomy Astrophys.* **419**, 777–782 (2004).
50. A. L. Yarin and E. Zussman, Upward needleless electrospinning of multiple nonofibers, *Polymer* **45**, 2977–2980 (2004).
51. M. Zrinyi and L. Szabo, Magnetic field sensitive polymeric actuators, *J. Intelligent Mater. Sys. Struct.* **9**, 667–671 (1998).
52. T.-Y. Liu, S.-H. Hu, K.-H. Liu, D.-M. Liu and S.-Y. Chen, Preparation and characterization of smart magnetic hydrogels and its use for drug release, *J. Magn. Magn. Mater.* **304**, e397–e399 (2006).
53. S. Bohlius, H. R. Brand and H. Pleiner, Surface waves and Rosensweig instability in isotropic ferrogels, *Z. Phys. Chem.* **220**, 97–104 (2006).

54. C. F. Hayes, Observation of association in a ferromagnetic colloid, *J. Colloid Interface Sci.* **52**, 239–243 (1975).
55. F. G. Baryakhtar, Yu. I. Gorobets, Ya. Kosachevskii, O. V. Il'chishin and P. K. Khizhenkov, Hexagonal lattice of cylindrical magnetic domains in thin ferrofluid films, *Magnitnaya Gidrodinamika* **3**, 120–123 (1981).
56. R. E. Rosensweig and J. Popplewell, Influence of concentration on field-induced phase transition in magnetic fluids, In *Electromagnetic forces and applications*, *Int. J. Appl. Electromag. Mater.*, **2** suppl., 83–86 (1992).
57. H. A. Stone and M. P. Brenner, Note on the capillary thread instability for fluids of equal viscosities, *J. Fluid Mech.* **318**, 373–374 (1996). The relaxation time in the viscous mode of instability is orders of magnitude slower than for inviscid breakup and hence dominates. Accordingly this estimate of interfacial tension corrects the value estimated in Ref. 56.
58. J.-C. Bacri, R. Perzynski, D. Salin, V. Cabuil and R. Massart, Phase diagram of an ionic magnetic colloid: experimental study of the effect of ionic strength, *J. Colloid Interface Sci.* **132**, 43–53 (1989).
59. A. O. Cebers, Thermodynamic stability of magnetofluids, *Magnetohydrodynamics* **18**, 137–142 (1982); see also Physical properties and models of magnetic fluids *Magnetohydrodynamics* **28**, 253–264 (1992). English translation.
60. K. Sano and M. Doi, Theory of agglomeration of ferromagnetic particles in magnetic fluids, *J. Phys. Soc. Japan* **52**, 2810–2815 (1983).
61. D. Lacoste and T. C. Lubensky, Phase transitions in a ferrofluid at magnetic-field-induced microphase separation, *Phys. Rev. E* **64**, 041506 (2001).
62. K. I. Morozov, A. F. Pshenichnikov, Yu. L. Raikher and M. I. Shliomis, Magnetic properties of ferrocolloids: The effect of interparticle interactions, *J. Magn. Magn. Mater.* **65**, 269–272 (1987).
63. V. Kalikmanov, Statistical thermodynamics of ferrofluids, *Physica A* **183**, 25–58 (1992).
64. A. F. Pshenichnikov and V. V. Mekhonoshin, Phase separation in dipolar systems: Numerical simulation, *JETP Letters* **72**, 182–185 (2000).
65. M. Klokkenburg, B. H. Erné, J. D. Meeldijk, A. Wiedenmann, A. V. Petukhov, R. P. A. Dullens and A. P. Philipse, In situ imaging of Field-Induced Hexagonal Columns in Magnetite Ferrofluids, *Phys. Rev. Lett.* **97**, 185702 (2006)
66. T. Tlusty and S. A. Safran, Defect-induced phase separation in dipolar fluids, *Science* **290**, 1328–1331 (2000).
67. Y. Zhu, C. Boyd, W. Luo, A. Cebers and R. E. Rosensweig, Periodic branched structures in a phase-separated magnetic colloid, *Phys. Rev. Lett.* **72**, 1929–1932 (1994).
68. A. T. Skjeltorp, One- and two-dimensional crystallization of magnetic holes, *Phys. Rev. Lett.* **51**, 2306–2309 (1983); Ordering phenomena of particles dispersed in magnetic fluids, *J. Appl. Phys.* **57**, 3285–3290 (1985).
69. J. B. Hayter, R. Pynn, S. Charles, A. T. Skjeltorp, J. Trewhella, G. Stubbs and P. Timmins, Ordered macromolecular structures in ferrofluid mixtures, *Phys. Rev. Lett.* **62**, 1667–1672 (1989).

70. J. Rabinow, The magnetic fluid clutch, *AIEE Transactions* **67**, 1308–1315 (1948).
71. P. Weissler, Cadillac magnetic-rheological shocks, *Popular Mechanics*, May (2000); see also M. R. Jolly, J. W. Bender and J. D. Carlson, Properties and applications of commercial magnetorheological fluids, Brochure. Lord Corporation, Cary, NC, USA.
72. W. I. Kordonsky *et al.*, Magnetorheological polishing devices and methods, US Patent 6,503,414 (2003); see also, N. Umehara and K. Kato, Hydromagnetic grinding properties of magnetic fluid containing grains at high speeds, *J. Magn. Magn. Mater.* **65**, 397–400 (1987).
73. J. Popplewell, R. E. Rosensweig and J. K. Siller, Magnetorheology of ferrofluid composites, *J. Mag. Mag. Mater.* **149**, 53–56 (1995); see also, J. Popplewell and R. E. Rosensweig, *J. Phys. D* **29**, 2297–2303 (1996).
74. R. E. Rosensweig, On magnetorheology and electrorheology as states of unsymmetric stress, *J. Rheology* **39**, 179–192 (1995).
75. M. Rasa, A. P. Philipse and D. Jamon, Initial susceptibility, flow curves, and magneto-optics of inverse magnetic fluids, *Phys. Rev. E* **68**, 031402.1–16 (2003).
76. R. V. Mehta, R. Patel, B. Chudesama, H. B. Desai, S. P. Bhatnagar and R. V. Upadhyay, Magnetically controlled storage and retrieval of light from dispersion of large magnetic spheres in a ferrofluid, *Current Science* **93**, 1071–1072 (2007); see also, J. N. Desai, Magnetic trapping of light, *Current Science* **93**, 452–453 (2007).
77. P. W. Anderson, Absence of diffusion in certain random lattices, *Phys. Rev.* **109**, 1492–1505 (1958).
78. S. John, Electromagnetic absorption in a disordered medium near a photon mobility edge, *Phys. Rev. Lett.* **53**, 2169–2173 (1984).
79. R. V. Mehta *et al.*, Effect of dielectric and magnetic contrast on photonic band gap in ferrodispersion, *Magnetohydrodynamics* **44**, 69 (2008).
80. M. Born and E. Wolf, Principles of optics: electromagnetic theory of propagation, interference and diffraction of light (Cambridge University, New York, 1999), 7th ed.
81. M. T. Lopez-Lopez, J. de Vicente, G. Bossis, F. Gonzalez-Caballero and J. D. G. Duran, Preparation of stable magnetorheological fluids based on extremely bimodal iron-magnetite suspensions, *J. Mater. Res.* **20**, 874–881 (2005).
82. R. E. Rosensweig, Theory for stabilization of magnetic colloid in liquid metal, *J. Mag. Mag. Mater.* **201**, Special issue, Proceedings of ICMF8, 1–6 (1999).
83. R. E. Rosensweig, G. R. Jerrauld and M. Zahn, Structure of magnetically stabilized fluidized beds in *Continuum Models of Discrete Systems 4*, O. Brulin and R. K. T. Hsieh, Eds.(North Holland, Amsterdam, 1981), pp. 137–144.
84. R. E. Rosensweig, Process concepts using field-stabilized two-phase fluidized flow, *J. Electrostat.* **34**, 163–187 (1995).

85. R. E. Rosensweig, Magnetic stabilization of the state of uniform fluidization, *Ind. Eng. Chem. Fundam.* **18**, 260–269 (1979).
86. R. E. Rosensweig, M. Zahn, W. K. Lee and P. S. Hagan, Theory and experiments in the mechanics of magnetically stabilized fluidized solids, in Theory of dispersed multiphase flow, R. E. Meyer, Ed. (Academic, New York, 1983).
87. R. E. Rosensweig and G. Ciprios, Magnetic liquid stabilization of fluidization in a bed of nonmagnetic spheres, *Powder Tech.* **64**, 115–123 (1991).
88. V. Cabuil and S. Neveu, Complex magnetic systems derived from magnetic fluids, In Magnetic fluids and applications handbook, Eds. B. Berkovski and V. Bashtovoi (Begell House, New York, 1996), pp. 56–63.
89. F. Brochard and P. G. de Gennes, Theory of magnetic suspensions in liquid crystals, *J. Phys. (Paris)* **31**, 691–708 (1974).
90. C. Y. Matuo, F. A. Torinho, M. H. Souza, J. Depeyrot and A. M. Figueredo-Neto, Lyotropic ferronematic liquid crystals based on new Ni, Cu, and Zn ionic magnetic fluids, *Brazilian J. Phys.* **32**, 458–463 (2002).
91. W. Wen, X. Huang and P. Sheng, Electrorheological fluids: structures and mechanisms, *Soft Matter* **4**, 200–210 (2008).
92. F. S. Bates and G. H. Fredrickson, *Physics Today* **52**, 32 (1999).
93. G. H. Fredrickson, The equilibrium theory of inhomogeneous polymers, (Oxford University, Oxford, 2005).
94. C. Park, J. Yoon and E. L. Thomas, *Polymer* **44**, 6725 (2003).
95. D. G. Bucknall, *Prog. Mat. Sci.* **49**, 713 (2004).
96. Y. A. Vlasov, X. Z. Bo, J. C. Sturm and D. J. Norris, *Nature* **414**, 289 (2001).
97. Y. Fink, J. N. Winn, S. Fan, C. Chen, J. Michel, J. D. Joannopoulos and E. L. Thomas, *Science* **282**, 1679 (1998).
98. A. K. Khandpur, S. Foerster, F. S. Bates, I. W. Hamley, A. J. Ryan, W. Bras, K. Almdal and K. Mortensen, *Macromolecules* **28**, 8796 (1995).
99. L. Leibler, *Macromolecules* **13**, 1602 (1980).
100. K. Binder, H. L. Frisch and S. Stepanow, *J. Phys. II (France)* **7**, 1353 (1997).
101. G. H. Fredrickson and E. Helfand, *J. Chem. Phys.* **87**, 697 (1987).
102. T. Ohta and K. Kawasaki *Macromolecules* **19**, 2621 (1986).
103. K. R. Shull, *Macromolecules* **25**, 2122 (1992).
104. M.W. Matsen and M. Schick, *Phys. Rev. Lett.* **72**, 2660 (1994).
105. K. Binder, *Acta Polymer* **46**, 204 (1995).
106. I. Szleifer, *Curr. Opin. Colloid. Sci.* **1**, 416 (1996).
107. Y. Tsori and D. Andelman, Thin film di-block copolymers in electric field: Transition from perpendicular to parallel lamellae, *Macromolecules* **35**, 5161–5170 (2002).
108. K. Amundson, E. Helfand, X. Quan and S. D. Smith, *Macromolecules* **26**, 2698 (1993); K. Amundson, E. Helfand, X. Quan, S. D. Hudson and S. D. Smith, *Macromolecules* **27**, 6559 (1994).
109. A. Onuki and J. Fukuda, *Macromolecules* **28**, 8788 (1995).
110. G. G. Pereira and D. R. M. Williams, *Macromolecules* **32**, 8115 (1999).
111. T. Thurn-Albrecht, J. DeRouchey and T. P. Russell, *Macromolecules* **33**, 3250 (2000).

112. A. V. Kyrylyuk, A. V. Zvelindovsky, G. J. A. Sevink and J. G. E. M. Fraaije, *Macromolecules* **35**, 1473 (2002).
113. A. Böker, A. Knoll, H. Elbs, V. Abetz, A. H.E. Müller and G. Krausch, *Macromolecules* **35**, 1319 (2002); A. Böker, K. Schmidt, A. Knoll, H. Zettl, H. Hansel, V. Urban, V. Abetz and G. Krausch, *Polymer* **47**, 849 (2006).
114. T. Xu, Y. Zhu, S. P. Gido and T. P. Russell, Electric field alignment of symmetric di-block copolymer thin films, *Macromolecules* **37**, 2625–2629 (2004).
115. V. Olszowka, M. Hund, V. Kuntermann, S. Scherdel, L. Tsarkova, A. Böker and G. Krausch, Large scale alignment of a lamellar block copolymer film via electric fields: a time resolved SFM study, *Soft Matter* **2**, 1089–1094 (2006).
116. K. Schmidt, H. G. Schoberth, M. Ruppel, H. Zettl, H. Hänsel, T. M. Weiss, V. Urban, G. Krausch and A. Böker, Reversible tuning of a block-copolymer nanostructure via electric fields, *Nature Matterials* **7**, 142–145 (2008).
117. M. W. Matsen, Electric-field alignment in thin films of cylinder-forming di-block copolymer, *Macromolecules* **39**, 5512 (2006).
118. C.-Y. Lin and M. Schick, Self-consistent-field study of the alignment by an electric field of a cylindrical phase of block copolymer, *J. Chem. Phys.* **125**, 034902 (2006).
119. T. Xu, A. V. Zvelindovsky, G. J. A. Sevink, O. Gang, B. Ocko, Y. Zhu, S. P. Gido and T. P. Russell, Electric field induced sphere-to-cylinder transition in di-block copolymer thin films, *Macromolecules* **37**, 6980–6984 (2004); T. Xu, C. J. Hawker and T. P. Russell, *Macromolecules* **38**, 2802 (2005).
120. Y. Tsori, F. Tournilhac, D. Andelman and L. Leibler, *Phys. Rev. Lett.* **90**, 145504 (2003).
121. Y. Tsori, D. Andelman, C.-Y. Lin and M. Schick, Block copolymers in electric fields: A comparison of single-mode and self-consistent field approximations, *Macromolecules* **39**, 289 (2006).
122. C.-Y. Lin, M. Schick, and D. Andelman, Structural changes of di-block copolymer melts due to an external electric field: a self-consistent field theory study, *Macromolecules* **38**, 5766 (2005).
123. J.-Y. Wang, T. Xu, J. M. Leiston-Belanger, S. Gupta and T. P. Russell, Ion complexation: a route to enhanced block copolymer alignment with electric fields, *Phys. Rev. Lett.* **96** 128301.1–4 (2006).